5 of 1

E86-10016

NASA-CR-176427

EVALUATION OF SPATIAL, RADIOMETRIC AND SPECTRAL THEMATIC MAPPER PERFORMANCE FOR COASTAL STUDIES

Submitted By

V. Klemas, S.G. Ackleson, M.A.-Hardisky
College of Marine Studies
University of Delaware
Newark, Delaware 19716

30 November 1985

Final Project Report
NASA Contract NAS-5-27580

Submitted To

H. Oseroff, Technical Monitor
NASA Goddard Space Flight Center
Code 902, Building 16
Greenbelt, Maryland 20771

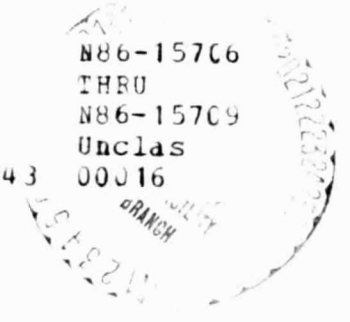

Summary

On 31 March 1983, the University of Delaware's Center for Remote Sensing initiated a study to evaluate the spatial, radiometric and spectral performance of the Landsat Thematic Mapper for coastal and estuarine areas. The investigation was supported by Contract NAS-5-27580 from the NASA Goddard Space Flight Center.

Our research was divided into three major subprojects. A summary of the results for each subproject is given below. Details of each subproject are described in the three attached papers.

1. A Comparison of Landsat TM to MSS Imagery for Detecting Submerged Aquatic Vegetation in Chesapeake Bay.

Landsat Thematic Mapper (TM) and Multispectral Scanner (MSS) imagery generated simultaneously over Guinea Marsh, Virginia, were assessed in the ability to detect submerged aquatic, bottom-adhering plant canopies (SAV). An unsupervised clustering algorithm was applied to both image types and the resulting classifications compared to SAV distributions derived from color aerial photography. Class confidence and accuracy were first computed for all water areas and then only shallow areas where water depth was less than six feet. In both the TM and MSS imagery, masking water areas deeper than six feet resulted in greater classification accuracy at confidence levels greater than 50%. Both systems performed poorly in detecting SAV with crown cover densities less than 70%. On the basis of the spectral resolution, radiometric sensitivity, and location of visible bands, TM imagery did not offer a significant advantage over MSS data for detecting SAV in lower Chesapeake Bay. However, because the TM imagery represents a higher spatial resolution, smaller SAV canopies may be detected than is possible with MSS data. Detailed results of this investigation are described in the attached paper (Ackleson and Klemas 1985).

2. Remote Sensing of Submerged Aquatic Vegetation: A Radiative Transfer Approach.

Radiative transfer theory was used to model upwelling radiance for an orbiting sensor viewing an estuarine environment. The environment was composed of a clear maritime atmosphere, an optically shallow estuary of either clear or turbid water, and one of three possible bottom types: vegetation, sand, or mud. Upwelling radiance was calculated for each case in TM bands 1, 2 and 3 and MSS bands 4 and 5 using data available in the literature. A spectral quality index was used to evaluate the relative effectiveness of TM and MSS bands in detecting submerged vegetation.

The effectiveness of an orbiting sensor in discriminating spectrally between submerged features is a function of the inherent contrast between the submerged features and how strongly the bottom signal is attenuated by the water column. In optically shallow water, the inherent contrast is the controlling factor. Thus, the optimum sensor band is that which correlates with the greatest inherent contrast between the submerged features. In the optically deeper water, the optimum sensor band is that for which the water column is most transparent.

In the clear ocean water, the optimum band for detecting vegetation on a sand or mud bottom is shown to change with the optical depth of the water. In the turbid San Vicente water, the optimum band in optically shallow water remains the optimum band in optically deeper water.

Under certain conditions, the spectral quality index will decrease to zero for some intermediate depth and then increase for yet deeper depths. This could have a significant impact upon how changes in water reflectance should be interpreted and can only be predicted with detailed knowledge of the spectral variation of optical parameters across the sensor band.

Radiometric calibration is shown to be a dominant factor in determining which TM or MSS band will be optimum for detecting a submerged feature such as SAV. Sensors with higher gain settings, in general, produce data with more information. The gain built into the TM sensors are significantly higher than those of the MSS, giving TM data a clear advantage for detecting submerged features. In several cases, a band is found to be optimum for detecting SAV in a radiometric sense, and yet sub-optimal in a spectral context.

The Thematic Mapper appears to be useful for detecting narrow SAV beds in the case of Broad Creek, Maryland. A nonparametric classification of a 2 November 1982 image clearly discriminated between SAV and the surrounding unvegetated bottom.

3. Remote Sensing of Coastal Wetland Biomass Using Thematic Mapper Wavebands.

Spectral data, simulating Thematic Mapper bands 3, 4 and 5 were gathered in salt and brackish marshes using a hand-held radiometer. Simple regression models were developed equating spectral radiance indices with total live biomass for S. alterniflora in a salt marsh and for a variety of plant species in a brackish marsh. Models were then tested using an independent set of data and compared to harvest estimates of biomass. In the salt marsh, biomass estimates from spectral data were similar to harvest biomass estimates during most of the growing season. Estimates of annual net aerial primary productivity calculated from spectral

data were within 21% of production estimated from harvest data. During August, biomass estimates from spectral data in the brackish marsh were similar to biomass estimated by harvesting techniques. At other times during the growing season, spectral data estimates of biomass were not always comparable to harvest biomass estimates. Reasonable estimates of wetlands biomass are possible during the peak of the growing season (August) using spectral data similar to Thematic Mapper bands 3, 4 and 5 gathered with hand-held radiometers.

4. General Results

Eleven journal articles and proceedings papers were produced during this research. They are listed on the following page. A detailed paper on each of the three subprojects is included in this report. During the course of this investigation, additional comparisons of TM and MSS were made for coastal applications. Results of a comparison of Landsat MSS, TM and simulated SPOT data for coastal application were presented at symposia and are described in several articles (Ackleson et al. 1985). Some of the results of this comparison are summarized in Table 1. Basically, the better spatial resolution of TM and SPOT offer major improvement for detecting many features in the coastal zone which tend to be narrow and long. This includes beds of submerged aquatic vegetation, submerged sand bars, pollution plumes, plots of marsh vegetation, etc. The Thematic Mapper offers additional improvements due to its superior spectral bands. TM band 1 is particularly important to studies of water properties and submerged features, while TM band 7 is very sensitive to moisture content of vegetation, which can be used as an indicator of plant vigor or stress. We have also found that all major wetland vegetation species can be clearly discerned in TM imagery. The spatial resolution of TM data appears to be better than 30 meters, i.e. it seems to be closer to 25 meters than 30 meters.

TABLE 1.

COMPARISON OF LANDSAT MSS

AND TM FOR COASTAL STUDIES

APPLICATION	IMPROVEMENT
Vegetation and Land Use Mapping	Medium
Biomass Measurement	Major
Submerged Aquatic Vegetation	Major
Eutrophication Phytoplankton Blooms	Medium
Suspended Sediment Currents, Turbidity Fronts	Medium
Pollution Plumes Ocean Dumping	Medium
Bathymetry Erosion Control	Major
Ship Traffic Harbor Planning	Major
Gross Coastal Geomorphology	Minor
Sargassum Open Ocean Fronts	Medium
Internal Waves Sea State	Minor

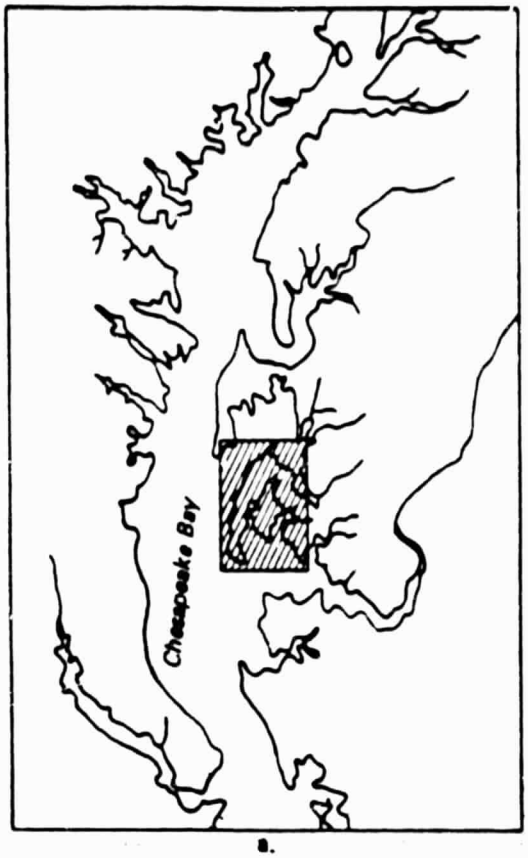

a.

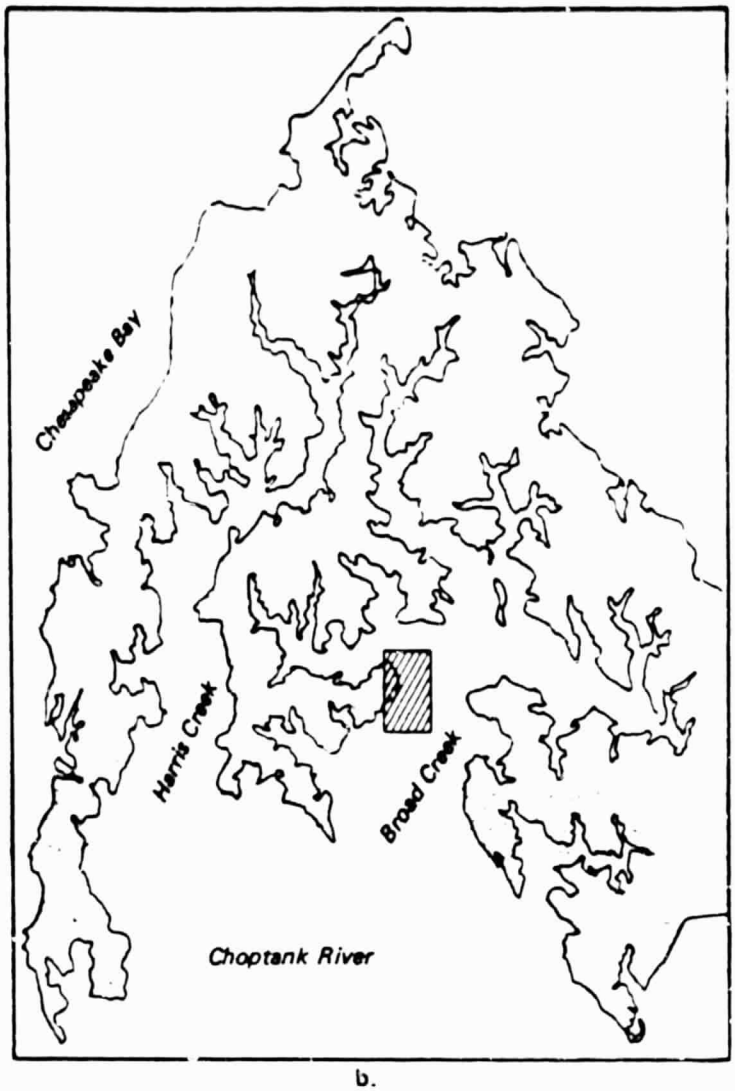

b.

FIGURE 5.

A portion of Chesapeake Bay is shown in plate a and an enlarged portion of Broad Creek, Maryland appears in plate b. The boxed area within plate b was photographed from low altitude on August 2, 1982. The photograph, plate c, shows a medium size SAV bed adjacent to the shoreline.

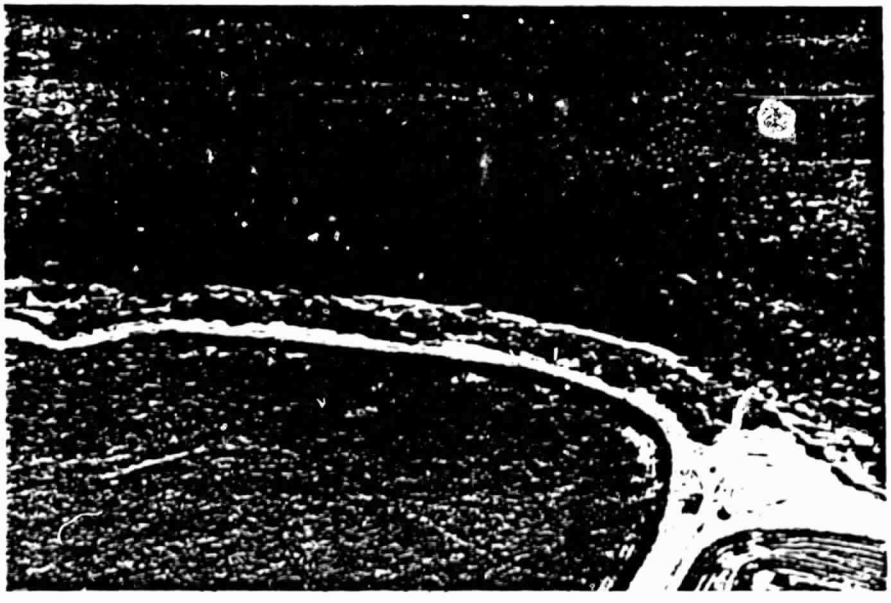

c.

5 of

E86-10016

NASA-CR-176427

EVALUATION OF SPATIAL, RADIOMETRIC AND SPECTRAL THEMATIC MAPPER PERFORMANCE FOR COASTAL STUDIES

Submitted By

V. Klemas, S.G. Ackleson, M.A.-Hardisky
College of Marine Studies
University of Delaware
Newark, Delaware 19716

30 November 1985

Final Project Report
NASA Contract NAS-5-27580

Submitted To

H. Oseroff, Technical Monitor
NASA Goddard Space Flight Center
Code 902, Building 16
Greenbelt, Maryland 20771

Summary

On 31 March 1983, the University of Delaware's Center for Remote Sensing initiated a study to evaluate the spatial, radiometric and spectral performance of the Landsat Thematic Mapper for coastal and estuarine systems. The investigation was supported by Contract NAS-5-27580 from the NASA Goddard Space Flight Center.

Our research was divided into three major subprojects. A summary of the results for each subproject is given below. Details of each subproject are described in the three attached papers.

1. A Comparison of Landsat TM to MSS Imagery for Detecting Submerged Aquatic Vegetation in Chesapeake Bay.

Landsat Thematic Mapper (TM) and Multispectral Scanner (MSS) imagery generated simultaneously over Guinea Marsh, Virginia, were assessed in the ability to detect submerged aquatic, bottom-adhering plant canopies (SAV). An unsupervised clustering algorithm was applied to both image types and the resulting classifications compared to SAV distributions derived from color aerial photography. Class confidence and accuracy were first computed for all water areas and then only shallow areas where water depth was less than six feet. In both the TM and MSS imagery, masking water areas deeper than six feet resulted in greater classification accuracy at confidence levels greater than 50%. Both systems performed poorly in detecting SAV with crown cover densities less than 70%. On the basis of the spectral resolution, radiometric sensitivity, and location of visible bands, TM imagery did not offer a significant advantage over MSS data for detecting SAV in lower Chesapeake Bay. However, because the TM imagery represents a higher spatial resolution, smaller SAV canopies may be detected than is possible with MSS data. Detailed results of this investigation are described in the attached paper (Ackleson and Klemas 1985).

2. Remote Sensing of Submerged Aquatic Vegetation: A Radiative Transfer Approach.

Radiative transfer theory was used to model upwelling radiance for an orbiting sensor viewing an estuarine environment. The environment was composed of a clear maritime atmosphere, an optically shallow estuary of either clear or turbid water, and one of three possible bottom types: vegetation, sand, or mud. Upwelling radiance was calculated for each case in TM bands 1, 2 and 3 and MSS bands 4 and 5 using data available in the literature. A spectral quality index was used to evaluate the relative effectiveness of TM and MSS bands in detecting submerged vegetation.

The effectiveness of an orbiting sensor in discriminating spectrally between submerged features is a function of the inherent contrast between the submerged features and how strongly the bottom signal is attenuated by the water column. In optically shallow water, the inherent contrast is the controlling factor. Thus, the optimum sensor band is that which correlates with the greatest inherent contrast between the submerged features. In the optically deeper water, the optimum sensor band is that for which the water column is most transparent.

In the clear ocean water, the optimum band for detecting vegetation on a sand or mud bottom is shown to change with the optical depth of the water. In the turbid San Vicente water, the optimum band in optically shallow water remains the optimum band in optically deeper water.

Under certain conditions, the spectral quality index will decrease to zero for some intermediate depth and then increase for yet deeper depths. This could have a significant impact upon how changes in water reflectance should be interpreted and can only be predicted with detailed knowledge of the spectral variation of optical parameters across the sensor band.

Radiometric calibration is shown to be a dominant factor in determining which TM or MSS band will be optimum for detecting a submerged feature such as SAV. Sensors with higher gain settings, in general, produce data with more information. The gain built into the TM sensors are significantly higher than those of the MSS, giving TM data a clear advantage for detecting submerged features. In several cases, a band is found to be optimum for detecting SAV in a radiometric sense, and yet sub-optimal in a spectral context.

The Thematic Mapper appears to be useful for detecting narrow SAV beds in the case of Broad Creek, Maryland. A nonparametric classification of a 2 November 1982 image clearly discriminated between SAV and the surrounding unvegetated bottom.

3. Remote Sensing of Coastal Wetland Biomass Using Thematic Mapper Wavebands.

Spectral data, simulating Thematic Mapper bands 3, 4 and 5 were gathered in salt and brackish marshes using a hand-held radiometer. Simple regression models were developed equating spectral radiance indices with total live biomass for S. alterniflora in a salt marsh and for a variety of plant species in a brackish marsh. Models were then tested using an independent set of data and compared to harvest estimates of biomass. In the salt marsh, biomass estimates from spectral data were similar to harvest biomass estimates during most of the growing season. Estimates of annual net aerial primary productivity calculated from spectral

data were within 21% of production estimated from harvest data. During August, biomass estimates from spectral data in the brackish marsh were similar to biomass estimated by harvesting techniques. At other times during the growing season, spectral data estimates of biomass were not always comparable to harvest biomass estimates. Reasonable estimates of wetlands biomass are possible during the peak of the growing season (August) using spectral data similar to Thematic Mapper bands 3, 4 and 5 gathered with hand-held radiometers.

4. General Results

Eleven journal articles and proceedings papers were produced during this research. They are listed on the following page. A detailed paper on each of the three subprojects is included in this report. During the course of this investigation, additional comparisons of TM and MSS were made for coastal applications. Results of a comparison of Landsat MSS, TM and simulated SPOT data for coastal application were presented at symposia and are described in several articles (Ackleson et al. 1985). Some of the results of this comparison are summarized in Table 1. Basically, the better spatial resolution of TM and SPOT offer major improvement for detecting many features in the coastal zone which tend to be narrow and long. This includes beds of submerged aquatic vegetation, submerged sand bars, pollution plumes, plots of marsh vegetation, etc. The Thematic Mapper offers additional improvements due to its superior spectral bands. TM band 1 is particularly important to studies of water properties and submerged features, while TM band 7 is very sensitive to moisture content of vegetation, which can be used as an indicator of plant vigor or stress. We have also found that all major wetland vegetation species can be clearly discerned in TM imagery. The spatial resolution of TM data appears to be better than 30 meters, i.e. it seems to be closer to 25 meters than 30 meters.

TABLE 1.

COMPARISON OF LANDSAT MSS

AND TM FOR COASTAL STUDIES

APPLICATION	IMPROVEMENT
Vegetation and Land Use Mapping	Medium
Biomass Measurement	Major
Submerged Aquatic Vegetation	Major
Eutrophication Phytoplankton Blooms	Medium
Suspended Sediment Currents, Turbidity Fronts	Medium
Pollution Plumes Ocean Dumping	Medium
Bathymetry Erosion Control	Major
Ship Traffic Harbor Planning	Major
Gross Coastal Geomorphology	Minor
Sargassum Open Ocean Fronts	Medium
Internal Waves Sea State	Minor

Publications (Articles and Papers)

Ackleson, S.G. and V. Klemas. 1983. Remote reconnaissance of submerged aquatic vegetation: A radiative transfer approach. Third Landsat-4 Workshop, NASA Goddard Space Flight Center, Greenbelt, MD, 6-7 December 1983.

Hardisky, M.A. and V. Klemas. 1983. Aboveground biomass estimation in a tidal brackish marsh using simulated Thematic Mapper spectral data. Third Landsat-4 Workshop, NASA Goddard Space Flight Center, Greenbelt, MD, 6-7 December 1983.

Ackleson, S.G. and V. Klemas. 1984. Assessing Landsat TM and MSS data for detecting submerged plant communities. Landsat-4 Science Characterization Early Results Symposium, NASA Goddard Space Flight Center, Greenbelt, MD, 23-24 February 1983. NASA Conference Publication 2355, IV:325-336.

Hardisky, M.A., F.C. Daiber, C.T. Roman and V. Klemas. 1984. Remote sensing of biomass and annual net aerial primary productivity of a salt marsh. Remote Sensing of Environment 16:91-106.

Hardisky, M.A. and V. Klemas. 1984. Remote sensing of coastal wetlands biomass using Thematic Mapper wavebands. Landsat-4 Science Characterization Early Results Symposium, NASA Goddard Space Flight Center, 23-24 February 1984. NASA Conference Publication 2355, IV:251-269.

Klemas, V. 1984. The use of remote sensing in estuarine and coastal resources management. NOAA Environmental Satellite User Symposium, Washington, DC, 26-28 March 1984.

Klemas, V. 1984. Remote sensing of coastal and ocean properties. Proceedings of SPIE: The International Society for Optical Engineering Technical Symposium East '84, Washington, DC, 29 April to 4 May 1984. Critical Reviews of Technology - Remote Sensing 475:42-54.

Ackleson, S.G., V. Klemas, H.L. McKim and C.J. Merry. 1985. A comparison of SPOT simulator data with Landsat MSS imagery for delineating water masses in Delaware Bay, Broadkill River and adjacent wetlands. Proceedings of 1984 SPOT Symposium, Scottsdale, AZ, 20-23 May 1984. Photogrammetric Engineering and Remote Sensing 51(8):1123-1129.

Ackleson, S.G. and V. Klemas. 1985. A comparison of Landsat TM and MSS imagery for mapping Zostera marina in Chesapeake Bay. NASA LIDQA Symposium, ASP/ACSM Fall Convention, Indianapolis, IN, 8-13 September 1985.

D1

N86-15707

A COMPARISON OF LANDSAT TM TO MSS IMAGERY FOR DETECTING SUBMERGED AQUATIC VEGETATION IN LOWER CHESAPEAKE BAY

BY

S. Ackleson
V. Klemas

College of Marine Studies
University of Delaware
Newark, Delaware

Presented At The 1985 ACSM-ASPRS Fall Convention
September 8-13, Indianapolis, Indiana

ABSTRACT

Landsat Thematic Mapper (TM) and Multispectral Scanner (MSS) imagery generated simultaneously over Guinea Marsh, Virginia are assessed in the ability to detect submerged aquatic, bottom-adhering plant canopies (SAV). An unsupervised clustering algorithm is applied to both image types and the resulting classifications compared to SAV distributions derived from color aerial photography. Class confidence and accuracy are first computed for all water areas and then only shallow areas where water depth is less than 6 feet. In both the TM and MSS imagery, masking water areas deeper than 6 Ft. resulted in greater classification accuracy at confidence levels greater than 50%. Both systems perform poorly in detecting SAV with crown cover densities less than 70%. On the basis of the spectral resolution, radiometric sensitivity, and location of visible bands, TM imagery does not offer a significant advantage over MSS data for detecting SAV in Lower Chesapeake Bay. However, because the TM imagery represents a higher spatial resolution, smaller SAV canopies may be detected than is possible with MSS data.

INTRODUCTION

Submerged aquatic vegetation (SAV) is believed to play a major role in the ecosystem of coastal, estuarine, and inland waters. In Chesapeake Bay, species such as Zostera marina (eel grass) provide food, shelter, and breeding areas for waterfowl, fish, shellfish, and many other forms of aquatic life. Because of the enormous commercial value of these areas, there exists a need to periodically assess the distribution and abundance of submerged aquatic plant communities.

Historically, data concerning SAV distribution and abundance has been acquired through exhaustive field sampling programs. Today, with the exception of very small scale studies, such surveys have become prohibitively expensive.

More recently, color aerial photography has been shown to provided much useful information for mapping SAV (Benton and Newnam, 1976; Austin and Adams, 1978; Macomber, 1981; Orth et al., 1979; Orth and Moore, 1981 and 1983). Orth et al. (1979) and Orth and Moore (1981) were able to document changes in the distribution and abundance of SAV at six sites within Chesapeake Bay from aerial photography dating back to 1937. Orth (1984) was able to map SAV density within Lower Chesapeake Bay from color aerial photography collected in 1979, 1980, 1982, and 1984. For each of these years, SAV distribution has been delineated on 1:24000 USGS topographic

quadrangles and classified according to apparent crown cover density; <10%, 10-40%, 40-70%, and 70-100%.

Most recently, remote sensing data gathered from orbiting platforms such as the LANDSAT series satellites has shown promise in delineating SAV. The degree to which these data may be used depends upon the configuration of the particular sensor; i.e. spatial and spectral resolution, band location, and radiometric sensitivity. Jensen et al. (1980) successfully used Landsat Multispectral Scanner (MSS) imagery to map kelp (Macrocystis pyrifera) along the California coast. The spatial resolution of MSS data is approximately 60 meters. Although the Landsat MSS collects data in four bands, two visible bands and two near infrared bands, only band 1 (500-600 nm) and band 2 (600-700 nm) are useful for detecting submerged features because water is an efficient absorber of IR radiation.

In 1983, NASA launched Landsat 4 equipped not only with a MSS but the first of a new series of scanners, the Thematic Mapper (TM). The spatial resolution of TM imagery is approximately 28 meters and 3 of the 7 available bands are located in the optical portion of the spectrum; band 1 (450-520 nm), band 2 (530-610 nm) and band 3 (620-690 nm). In addition, the radiometric sensitivity of the TM is as much as 3 times that of the MSS (Table 1). All of these attributes suggest that TM imagery should contain more submerged features information than MSS data. The purpose of this work is to compare the relative capability of TM imagery with MSS

data for detecting SAV within Lower Chesapeake Bay. The comparison is based upon SAV distribution derived by Orth from color aerial photography collected 28 days prior to the LANDSAT overpass.

DESCRIPTION OF STUDY AREA

The area of interest is located in Lower Chesapeake Bay, at the mouth of the York River, along the southern shore of Mobjack Bay (Figure 1). The area encompasses 41.1 km^2, approximately 6.5 km^2 of which is inhabited by SAV. These bottom-adhering canopies are composed mostly of Zostera marina and Ruppia maritima and are typically situated in shallow water adjacent to the shoreline. During the summer, both of these species are abundant with Ruppia occupying the most shallow areas (<.5m) and Zostera dominating deeper areas to a depth of about 1.5m. During the winter, the SAV distribution and abundance decreases as the Ruppia practically disappears and the Zostera dies back significantly.

The bottom substrate throughout the study area is composed of bright sand. From the air, the sav canopies appear as dark patches upon an otherwise bright bottom.

The water clarity varies seasonally with most clear conditions occurring in the winter months. During the summer, higher nutrient concentrations, warmer water, and increased surface light

intensities, often induce plankton blooms. The resulting turbidity may greatly reduce the ability of an observer or remote sensing device to detect SAV. Van Tine and Wetzel (1983) reported seasonal averages of irradiance attenuation measured at several sites in Lower Chesapeake Bay containing SAV. Their data indicate that during the winter, the average depth at which the downwelling light intensity has decreased to 1% of the surface intensity for blue (410 nm), green (540 nm) and red (671 nm) light is, respectively, 2.0 m, 5.7 m, and 3.2 m. During the summer, the mean attenuation depth decreases to about 0.8 m, 1.9 m, and 1.6 m for blue, green and red light, respectively.

The tidal range throughout the Guinea Marsh area is approximately 1 meter. Given the relatively turbid water conditions, especially during the summer, remote sensing of SAV should be conducted as close to low tide as possible.

METHODOLOGY

Landsat TM and MSS imagery generated simultaneously over the study area was classified using an unsupervised clustering algorithm. All data analysis was performed using an ERDAS 400 computer system. The input parameters governing the operation of the clustering program are defined as functions of the TM and MSS system noise. The classified TM and MSS imagery are then compared, pixel-

by-pixel, to digitized SAV distributions delineated from color aerial photography. Class confidence and accuracy are calculated for each scene and used as a basis for comparing the two image types.

LANDSAT Imagery

LANDSAT TM and MSS imagery of the Guinea Marsh area was generated simultaneously on July 19, 1984. At the time of the overpass, 1009 local time, the sky was cloud-free and reasonably clear of haze. The solar zenith angle was 32°. The tide at Guinea Marsh was flooding and low tide occurred at 0706 local time.

Prior to classification, each image was geometrically corrected and registered to a USGS topographic quadrangle of the Guinea Marsh area. The TM image was resampled to simulate 28 meter resolution and the MSS data was resampled to simulate 60 meter resolution.

Reference SAV Maps

Since 1978, the Virginia Institute of Marine Science has conducted annual and biannual surveys of SAV distribution within Lower Chesapeake Bay (Orth and Moore, 1983). In each survey, 1:24000 color aerial photography was collected during the summer months. The photography was then classified into several catagories of SAV using visual interpretation techniques. SAV catagories are based

upon spatially averaged crown densities and expressed as a percent coverage or crown cover; 0-10%, 10-40%, 40-70%, and 70-100%. The SAV delineations were then transferred to 1:24000 USGS topographic quadrangles. The 1984 survey, conducted on June 21, 1984, 28 days prior to the Landsat Overpass, is used here as a reference with which to compare the classified TM and MSS imagery. A TM reference image is created by digitizing the SAV map, using a CALCOMP 9100 digitizer, to simulate 28 meter resolution. To create the MSS reference image, the SAV map is digitized to simulate 60 meter resolution. In both cases, the image/SAV map registration accuracy is ±1 pixel.

Landsat TM And MSS Image Clustering

The image clustering algorithm, CLUSTER, was developed by ERDAS Inc. and is based upon a program formulated by NASA/JSC as part of the ASTEP software package (ERDAS 400 Image Processing and Geographic Information System User's Guide, 1983). CLUSTER is a two-pass unsupervised classifier designed to group pixels of a multi-band image into N number of spectral classes. In the first pass, the operator defines the maximum cluster radius (R), the minimum Euclidean distance in P-space between cluster centroids (D), where P is the number of spectral bands in the image, and the maximum number of classes to be produced (N). The program considers each pixel in a sequential manner, starting at the upper left corner of the scene and progressing line-by-line to the lower right corner.

Class mean vectors, generated in the first pass, are used in the second pass, wherein a minimum distance classifier is applied to the entire image.

One disadvantage to using an unsupervised classifier such as CLUSTER is the relatively small amount of control that the operator has over the program. Because image classification is a function of the input variables, the operator must have some prior knowledge of the scene variance in order to select reasonable values of R, D and N. In this work, it is also necessary to standardize the selection of input values in order to provide a basis for comparison between the classified TM and MSS imagery.

As an image is generated by either the TM or the MSS, system noise is introduced, primarily as a result of differences in detector calibration, voltage fluctuations within the satellite, and round off error in the digitization process. The effect of this noise is to limit the ability of the sensor to detect more subtle variations in scene radiance than would normally be detected if the image were noise-free. Within any classification, no matter how sophisticated the classifier, classes will be meaningful only if the spectral separation from other classes is greater than the system noise.

The maximum cluster radius and minimum distance between clusters are defined as functions of the system noise as

$$R = \sigma_S \quad (1)$$

and

$$D = 2R , \quad (2)$$

where σ_S^2 is the variance in count values as a result of system noise. The system noise variance may be estimated for each image band by calculating σ^2 within a homogeneous region of the image. The more homogeneous the region and the larger the number of pixels within the region, the better the estimate of σ_S^2. Within both the TM and MSS imagery, optically deep water appeared to be most homogeneous and geographically similar areas were selected within each image for the estimate of σ_S^2. Within the TM image the area comprised 90 pixels while, in the MSS image, 20 pixels were represented. Values of R and D used to classify the TM and MSS imagery are shown in Table 2.

For each classification, N=50, the maximum number of classes that CLUSTER can create. However, classification error can occur when actual number of classes created is N. This will most likely be the case when the selected values of R and D are small relative to the variance in count values throughout the scene. When the maximum number of clusters is reached, new clusters may not be created until two or more of the existing classes are aggregated. Within the TM and MSS scenes, the majority of scene variance occurs within land areas. Therefore, prior to running the classifier,

all land areas within both images were masked using one of the IR bands - TM band 4 (770-900 nm) and MSS band 4 (800-1100 nm). This caused the classifier to assign just 1 class to land and allowed as many as 49 water classes to be created.

Calculation Of Confidence And Accuracy

The classified TM and MSS images are compared pixel-by-pixel with the digitized, 1984 SAV distribution map of Guinea Marsh. For each class, confidence and accuracy are calculated, where

$$\text{Confidence} = \frac{\text{\# Correctly Classified Pixels}}{\text{\# Pixels Within Class}} \qquad (3)$$

and

$$\text{Accuracy} = \frac{\text{\# Correctly Classified Pixels}}{\text{\# SAV Map Pixels}} \quad . \qquad (4)$$

Within each class, a pixel is correctly classified if it correlates with a SAV pixel within the reference image.

TM and MSS classification confidence and accuracy was first computed for all water areas. Next, all water areas deeper than 6 feet were masked within the TM and MSS classifications using NOAA chart 12238, published in 1979, digitized and registered to each image. Class confidence and accuracy was then recalculated and compared with the values representing all water areas.

RESULTS AND DISCUSSION

Classification accuracies computed for all water areas indicate no significant difference between TM and MSS imagery for detecting SAV in the Guinea Marsh area (Table 3). Both data types performed poorly in discriminating SAV canopies having crown cover densities of 0-10%, 40-70%, and 70-100%. In the latter case, classification accuracies appeared to increase within the 50-75% and 75-100% confidence intervals, but the increases were too small to be considered significant.

There appeared to be moderate success in detecting SAV crown cover densities of 10-40%. This was a somewhat surprising result as classification accuracies were expected to increase with SAV density. To further investigate this result, all pixels having a classification confidence ≥50% were highlighted within the unclassified TM and MSS imagery. A high correlation was found between these pixels and bright areas within the imagery.

For any plant canopy, the volume reflectance may be divided into 2 components; that light which is reflected from the plant material and that light which is reflected from the underlying substrate. When the canopy is dense (i.e. crown cover densities approaching 100%), the first component dominates the volume reflectance of the canopy. As the plant density decreases, the second

component increases. Within the Guinea Marsh area, the substrate is composed of bright sand and dense SAV canopies appear from the air as dark areas upon an otherwise bright bottom. The fact that pixels classified with high confidence for the 10-40% SAV crown cover correlate with bright areas within the unclassified imagery indicates that the classifier is not discriminating SAV, but rather shallow sandy areas. Although aerial photography indicated a 10-40% SAV crown cover, the TM and MSS scene radiance is dominated by reflectance from the bright, sandy substrate.

When all water areas of depth ≥6 feet are eliminated from the classification analysis, accuracies for the 50-75% and 75-100% confidence intervals were found to increase only for SAV of crown cover density 70-100% (Table 4). For the 75-100% confidence interval, TM classification accuracy increased from 0.2% to 19.7%. MSS classification accuracies increased similarly; 0.5% to 13.3%. All other accuracies remained unchanged for confidence levels greater than 50%. This indicates that within both TM and MSS imagery, it is difficult to distinguish between Lower Chesapeake Bay SAV and optically deep water. More importantly, by masking optically deep water, classification accuracies associated with high confidence levels may be increased significantly.

The only advantage that TM imagery appears to have over MSS data within this study is the ability to detect smaller canopies and more clearly delineate larger canopies. The higher spatial

resolution of TM imagery could further increase in importance for study areas located in Upper Chesapeake Bay where the SAV canopies tend to be smaller and less numerous than in the Lower Chesapeake Bay.

CONCLUSIONS

Landsat TM and MSS imagery are similarly effective in detecting SAV in Lower Chesapeake Bay occupying bright, sandy substrates. The increased radiometric sensitivity and spectral resolution and the addition of a third optical band does not afford TM imagery a significant advantage over MSS data. However, the reader is advised against extending this conclusion to other topics in water research or, for that matter, SAV occupying substrates having a spectral reflectance more closely resembling the canopy. For cases in which spectrally similar water masses are to be delineated or when SAV is to be detected upon dark, muddy substrates, the radiometric and spectral characteristics of the TM bands may offer a significant improvement over those of the MSS.

The only apparent advantage to using TM imagery over MSS data for detecting SAV in Lower Chesapeake Bay is that, by virtue of higher spatial resolution, smaller SAV canopies may be detected.

REFERENCES

Austin, A. and R. Adams. 1978. Aerial color and color infrared survey of marine plant resources. Photogrammetric Engineering and Remote Sensing. Vol. 44, No. 4, Pp. 469-480.

Benton, A.R. and R.M. Newnam. 1976. Color aerial photography for aquatic plant monitoring. Journal of Aquatic Plant Management. Vol. 14, Pp. 14-16.

ERDAS Image Processing and Geographic Information System User's Guide. 1983. ERDAS Inc., 999 McMillan Street N.W., Atlanta, Georgia.

Jensen, J.R., J.E. Estes and L. Tinney. 1980. Remote sensing techniques for Kelp surveys. Photogrammetric Engineering and Remote Sensing. Vol. 46, No. 6, Pp. 743-755.

Macomber, R.T. 1981. Mapping submerged aquatic vegetation in Chesapeake Bay. In: G. Belie and P. Cornillion (eds.). Remote sensing, a tool for managing the marine environment: Eight case studies. University of Rhode Island Marine Technical Report 77.

Orth, R.J., K.A. Moore and H.H. Gordon. 1979. Distribution and abundance of submerged aquatic vegetation in Lower Chesapeake Bay, Virginia. Final Report to USEPA. Chesapeake Bay Program. EPA-600/8-79-029/SAVI.

Orth, R.J. and K.A. Moore. 1981. Submerged aquatic vegetation of the Chesapeake Bay: past, present and future. Trans. 46th North American Wildlife and Reserve Conference. Pp. 271-283.

Orth, R.J. and K.A. Moore. 1983. Submerged vascular plants: Techniques for analyzing their distribution and abundance. Marine Technology Society Journal. Vol. 17, No. 2, Pp. 38-52.

Orth, R.J. 1984. Personal communication.

Stevenson, J.C. and N.M. Confer. 1978. Summary of available information on Chesapeake Bay submerged vegetation. FWS/OBS-78/66. U.S. Fish and Wildlife Service, Annapolis, Maryland. 333 p.

Van Tine, R.F. and R.L. Wetzel. 1983. Structural and functional aspects of the ecology of submerged aquatic macrophyte communities in the Lower Chesapeake Bay; Volume II; Submarine light quantity and quality in the Lower Chesapeake Bay and its potential role in the ecology of submerged grass communities. Special Report No. 207. Applied Marine Science

and Ocean Engineering, Virginia Institute of Marine Studies, Gloucester Point, Virginia.

Wetzel, R.L. 1983. Structural and functional aspects of the ecology of submerged aquatic macrophyte communities in the Lower Chesapeake Bay; Volume I; Studies on structure and function of a temperate, estuarine seagrass community: Vaucluse Shores, Lower Chesapeake Bay, Virginia, U.S.A. Special Report No. 267. Applied Marine Science and Ocean Engineering, Virginia Institute of Marine Studies, Gloucester Point, Virginia.

Table 1.

Radiometric Sensitivity[1] Of Optical TM And MSS Bands

Band	Wavelength Region (nm)	Gain	Offset
MSS1	500-600	5.570	-1.114
MSS2	600-700	7.216	-2.886
TM1	450-520	15.944	2.423
TM2	530-610	8.199	2.329
TM3	620-690	10.814	1.265

[1] COUNT = GAIN * L + OFFSET
COUNT = 0-255
GAIN = COUNT/mwcm$^{-2}\mu m^{-1}str^{-1}$
L = SCENE RADIANCE
OFFSET = 0-255

Table 2.

Maximum Cluster Radius (R) And Minimum Between-Cluster Distance (D) Used To Classi. y The TM and MSS Imagery

	TM	MSS
R	.903	.580
D	1.806	1.160

Table 3.

Landsat TM and MSS Classification
Accuracies For All Water Areas

% SAV Crown Cover	Sensor	Confidence 0-25%	25-50%	50-75%	75-100%
0-10	TM	100.0	0.0	0.0	0.0
	MSS	97.3	2.7	0.0	0.0
10-40	TM	72.1	17.5	9.2	1.2
	MSS	76.2	8.3	15.5	0.0
40-70	TM	100.0	0.0	0.0	0.0
	MSS	92.4	7.6	0.0	0.0
70-100	TM	98.5	1.2	0.1	0.2
	MSS	96.7	1.8	1.0	0.5

Table 4.

Landsat TM and MSS Classification Accuracies
For Water Areas Less Than 6 Feet

% SAV Crown Cover	Sensor	Confidence 0-25%	25-50%	50-75%	75-100%
0-10	TM	100.0	0.0	0.0	0.0
	MSS	97.3	2.7	0.0	0.0
10-40	TM	72.1	17.5	9.2	1.2
	MSS	76.2	8.3	15.5	0.0
40-70	TM	99.9	0.1	0.0	0.0
	MSS	82.9	17.1	0.0	0.0
70-100	TM	53.6	16.7	10.0	19.7
	MSS	55.9	15.7	15.1	13.3

D2

REMOTE RECONNAISSANCE OF SUBMERGED AQUATIC VEGETATION: A RADIATIVE TRANSFER APPROACH

Steven G. Ackleson
Vytautas Klemas

N86-15708

College of Marine Studies
University of Delaware
Newark, Delaware 19711

1. INTRODUCTION

This research is concerned with assessing the effectiveness of LANDSAT TM and MSS sensors for detecting submerged aquatic vegetation (SAV). We approach the problem from a theoretical standpoint in which we simulate volume reflectance from SAV under a variety of conditions. Here, we focus upon the spectral and radiometric qualities of TM bands 1, 2 and 3 and MSS bands 4 and 5.

2. BACKGROUND

The vast majority of remote sensing research involved with detecting surface features addresses the problem in a purely stochastic fashion. Typically, computers are used to generate categories within digital multi-band data based upon spectral signatures. Signatures may be derived either manually by selecting subsets of data that correlate with ground observations or by instructing the computer to group similar signatures. The image is then classified by statistically assigning each pixel to one of the categories. These techniques are nonparametric in the sense that the classifier makes no assumptions about the physical characteristics of surface features. Under certain conditions, e.g. large, homogeneous surface features relative to the spatial resolution of the sensor, the nonparametric approach has been very successful. Numerous examples are available in the literature and Moik (1980) gives a good overview of the subject.

In a parametric approach, the researcher attempts to predict upwelling radiance at an airborne or orbiting sensor by modeling radiative transfer. The problem becomes significantly more complicated because the researcher requires knowledge of the transmittance and reflectance characteristics of the surface feature as well as the atmosphere. The advantage of the parametric approach is that the researcher gains valuable insight for interpreting observed radiance changes in the imagery.

3. METHODOLOGY

3.1 Spectral Assessment

Radiative transfer theory is used to model upwelling radiance that would be received by LANDSAT TM and MSS viewing a hypothetical estuarine

---

Presented at the Third Landsat-4 Workshop, NASA Goddard Space Flight Center, Greenbelt, MD, 6-7 December 1983.

environment, shown in Figure 1. The environment is composed of a clear maritime atmosphere, an optically shallow estuary of either clear or turbid water, and three possible bottom types: vegetation, sand or mud.

3.1.1 The Atmosphere

A clear maritime air mass is selected and is described by Guttman (1968). Using solar irradiance data (Gast et al., 1965) as input, solar and sky irradiance is calculated at sea level as well as path radiance that would be received by an orbiting sensor. These calculations assume a solar zenith angle of 50^0.

3.1.2 The Water Column

Irradiance reflectance of the water column and bottom is calculated using a quasi-single scattering model developed by Philpot (1981).

$$R_I = \frac{B_d}{K_t}(1-e^{-K_t d}) + A_b e^{-K_t d} \qquad (1)$$

Where R_I = irradiance reflectance of the water and bottom,

B_d = irradiance backscatter coefficient,

K_t = total irradiance attenuation coefficient (the sum of the attenuation coefficients for upwelling and downwelling irradiance),

d = water depth,

A_b = irradiance reflectance of the bottom.

Equation (1) is used, at the expense of slightly lower accuracy, rather than a two-flow or Monte Carlo approach because the two necessary terms, B_d and K_t, are easily calculated from simple field measurements available in the literature and the amount of computer time required is relatively small.

The water column is assumed to be vertically homogeneous and the water surface calm and flat. Two very different water qualities are considered; clear ocean water and turbid fresh water. Measurements representing clear oceanic water are documented in Tyler et al. (1972). Measurements representing very turbid water were made in San Vincente, a man-made lake northeast of San Diego, and are documented in Tyler and Smith (1970). Calculated values of B_d and K_t for both water types are shown in Table 1.

3.1.3 The Bottom Types

Three different reflectance profiles are selected from the literature to represent a submerged plant canopy, sand and mud. The spectral reflectance of each bottom type is shown in Figure 2.

3.1.4 Upwelling Radiance Above the Earth

The upwelling radiance that would be received by an orbiting sensor is calculated as:

$$L_{os} = [H_o R_I + P_a L_d] T_o + L_p , \quad (2)$$

L_{os} = upwelling radiance at the orbiting sensor,

H_o = the combined effects of the atmosphere and air/water interface upon radiance reflected from the water,

R_I = irradiance reflectance of the water and bottom,

P_a = Fresnel reflectance of downwelling radiance at the water surface,

L_d = downwelling sky radiance,

T_o = optical thickness of the atmosphere in the zenith direction, and

L_p = atmospheric path radiance received by the sensor.

Upwelling radiance values are calculated every 10 nm over the wavelength range 450 nm to 700 nm. Radiance values are then summed over TM bands 1 (450-520 nm), 2 (520-600 nm), and 3 (630-690 nm) and MSS bands 4 (500-600 nm) and 5 (600-700 nm).

3.1.5 Spectral Quality Index

A spectral quality index is defined based upon the work of Lyzenga and Polcyn (1978) as:

$$SQI = |L_T - L_B| \; L_B^{-1/2} \quad (3)$$

where:

L_T = upwelling radiance representing the submerged plant canopy, and

L_B = upwelling radiance representing a background of sand or mud.

Equation (3) is quite similar to the equation for apparent contrast. Relative values of SQI between bands indicate relative effectiveness in detecting submerged plant canopies.

3.2 Radiometric Assessment

The radiometric resolutions of TM bands 1, 2 and 3 and MSS bands 4 and 5 are compared for the same cases discussed in the previous section. Upwelling radiance at satellite altitude calculated for each band is converted to count values using calibrations taken from Barker et al.

(1983) for TM sensors and Bauer (1980) for LANDSAT-3 MSS sensors (see Table 2 for conversion constants). Apparent contrast is then calculated between target and background signals as:

$$\Delta C = |C_T - C_B|$$

where

C_T = count value calculated from target signal, and

C_B = count value calculated from background signal.

3.3 Quick-Look Evaluation of TM Data

An ERDAS 400 microcomputer is used to enhance and classify a TM image of Broad Creek, Maryland. The image was generated on November 2, 1982. The scene is classified using an unsupervised clustering routine. The classified scene is compared with aerial photography of the area collected on August 2, 1982. Of primary interest in the scene is a medium size SAV bed located on the west bank of Broad Creek, latitude 38°44'20"N, longitude 76°15'25"W. The SAV was photographed from a Cessna 174 at low altitude using a hand-held camera and Kodak Pan-X black and white film.

4. RESULTS

SQI values are calculated for clear water overlying a sand bottom, clear water overlying a mud bottom, turbid water overlying a sand bottom, and turbid water overlying a mud bottom. The results are shown in Tables 3-5 respectively. In all cases, when the water depth is optically shallow TM band 3 and MSS band 5 are most effective in detecting the submerged vegetation. This is intuitively correct since the inherent contrast between the vegetation and both the sand and mud is a maximum in these two bands. In clear water, as the water depth increases, the optimum band shifts from TM band 3 and MSS band 5 to TM band 1 for both bottom types. Here, the attenuation of bottom signal is less in TM band 1 than in TM band 3 and MSS band 5. In turbid water the relative effectiveness of each band is similar for all depths considered.

Spectrally, MSS band 4 is quite similar to TM band 2 and MSS band 5 is similar to TM band 3. Nevertheless, some unanticipated changes in relative SQI values between these bands are observed with respect to increasing water depth. Shown in Table 5, MSS band 4 is slightly more effective than TM band 2 in discriminating between submerged vegetation and sand at 0.5 meters. When the water depth increases to 1.5 meters, TM band 2 becomes slightly more effective. Similar results are seen in Tables 2 and 3 between TM bands 3 and MSS band 5.

In most cases, SQI values decrease with increasing depth. This also seems intuitively correct as the apparent contrast decreases with either increasing attentuation or increasing pathlength. In Table 4, SQI decreases in TM band 2 between 0.5 and 1.5 meters and then increases

between 1.5 meters and 10.0 meters. To understand what is happening here it is necessary to know something about the variation in the optical characteristics of the water and the bottom types across the band. Figure 3 shows the spectral reflectance of the vegetation and mud within TM band 2. Whereas the largest reflectance from the vegetation occurs in the shorter wavelength portion of the band, the reflectance of the mud increases toward the longer wavelength region. The average reflectance of the mud is slightly larger than the vegetation so that in the absence of a water column, the mud would appear brighter. Also shown in Figure 3 is the total attenuation coefficient of the clear ocean water which increases significantly toward the longer wavelength region of the band. Under these circumstances, the signal from the mud decreases rapidly with increasing water depth than does the vegetation signal. Figure 4 is a plot of SQI without taking the absolute value of the numerator. Values were calculated for several depths between 0 and 20 meters. In very shallow water, the signal from the mud is greater than the signal from the vegetation and the index takes on a negative value. At some intermediate depth slightly greater than 1.0 meters, the two signals are equal and SQI is zero. At still greater depths the vegetation appears brighter than the mud and SQI values are positive. As the depth becomes very deep, both signals take on the value of optically deep water and SQI again falls to zero. This emphasizes the importance of making optical measurements within natural waters at appropriate spectral resolutions. If all optical measurements were made with a broad band radiometer representing TM band 2, the intermediate zero contrast would never have been noticed and the model predictions of upwelling radiance would have been in gross error.

Also shown in Tables 3-6 are apparent contrast calculations in which upwelling radiance is converted to count values. The results simulate the absolute count difference within the satellite image between pixels representing the SAV and those representing the surrounding unvegetated sand or mud. For the case of clear ocean water, TM band 1 offers the best discrimination between the SAV and the background, both sand and mud. This result does not agree with that of the SQI analysis, the reason being that each sensor has a unique counts-to-radiance calibration. In Table 2, the higher the sensor gain, the more sensitive it is to changes in reflectance. Thus, even though spectrally TM band 3 is better than TM band 1, the larger gain of TM band 1 more than makes up for the difference. This same effect occurs between TM bands 2 and 3 and the spectrally similar MSS bands 4 and 5. In each case the gain is larger for the TM bands, making them significantly more efficient in detecting the SAV.

A TM band 5 image of Broad Creek, Maryland is shown in Figure 5a. The image was generated on November 2, 1983. Figure 5b shows an aerial photograph of a SAV bed located along the west shore of Broad Creek. The SAV appears as a dark area adjacent to the shoreline on an otherwise bright bottom. The photo was taken on August 2, 1982, three months prior to the TM image. The TM image is classified with an unsupervised clustering routine using an ERDAS 400 microcomputer. The classified image is shown in Figure 6. The area classified as SAV correlates well with that shown in the aerial photography.

5. CONCLUSIONS

The effectiveness of an orbiting sensor in discriminating spectrally between submerged features is a function of the inherent contrast between the submerged features and how strongly the bottom signal is attenuated by the water column. In optically shallow water the inherent contrast is the controlling factor. Thus, the optimum sensor band is that which correlates with the greatest inherent contrast between the submerged features. In optically deeper water, the optimum sensor band is that for which the water column is most transparent.

In the clear ocean water the optimum band for detecting vegetation on a sand or mud bottom is shown to change with the optical depth of the water. In the turbid San Vicente water the optimum band in optically shallow water remains the optimum band in optically deeper water.

Under certain conditions the spectral quality index will decrease to zero for some intermediate depth and then increase for yet deeper depths. This could have a significant impact upon how changes in water reflectance should be interpreted and can only be predicted with detailed knowledge of the spectral variation of optical parameters across the sensor band.

Radiometric calibration is shown to be a dominant factor in determining which TM or MSS band will be optimum for detecting a submerged feature such as SAV. Sensors with higher gain settings in general produce data with more information. The gain built into the TM sensors are significantly higher than those of the MSS, giving TM data a clear advantage for detecting submerged features. In several cases, a band is found to be optimum for detecting SAV in a radiometric sense and yet sub-optimal in a spectral context.

The Thematic Mapper appears to be useful for detecting SAV in the case of Broad Creek, Maryland. A nonparametric classification of a November 2, 1982 image clearly discriminated between SAV and the surrounding unvegetated bottom.

6. REFERENCES

Austin, R., 1974. The remote sensing of spectral irradiance from below the ocean surface. In Optical Aspects of Oceanography. Jerlov and Nielsen, Editors. Academic Press, New York. pp. 317-343.

Barker, J. L., D. L. Ball, K. C. Leung and J. A. Walker, 1983. Prelaunch absolute radiometric calibration of the reflective bands on LANDSAT-4 protoflight thematic mapper. LANDSAT-4 Scientific Characterization Early Results Symposium. NASA/Goddard Space Flight Center, Greenbelt, Maryland, 20771.

Bauer, B. P. Personal communication. September 18, 1980. Geological Survey, EROS Data Center, Sioux Falls, South Dakota, 57198.

Cast, P. R., 1965. Solar electromagnetic radiation: solar irradiance. In Handbook of Geophysics and Space Environments. S. L. Valley, Editor. McGraw-Hill Publishing Company, New York. pp. 1-16.

Gates, D. M., H. J. Keegan, J. C. Schleter, and V. R. Weidner, 1965. Spectral properties of plants. Applied Optics. Vol. 4, No. 1, pp. 11-20.

Guttman, A., 1968. Extinction coefficient measurements on clear atmospheres and within clouds. Applied Optics. Vol. 7, No. 12, pp.2377-2381.

Moik, Johannes G., 1980. Digital Processing of Remotely Sensed Images. NASA SP-431, 330 p.

Lyzenga, D. R. and F. C. Polcyn, 1978. Analysis of optimum spectral resolution and band location for satellite bathymetry. NASA Final Report on Contract 7-35176. 59 p.

Lyzenga, D. R. and F. Thomson, 1978. Basic remote sensing investigation for beach reconnaissance - bottom features task force. ONR Final Report on Contract N0014-74-C-0273. 36 p.

Philpot, W., 1981. A radiative transfer model for remote sensing of vertically inhomogeneous waters. Doctoral Dissertation, College of Marine Studies, University of Delaware, Newark, Delaware, 19716. 140 p.

Tyler, J. E., R. C. Smith and W. H. Wilson, 1972. Predicted optical properties of clear natural water. Journal of the Optical Society of America, Vol. 62, No. 1, pp. 83-91.

Tyler, J. E. and R. C. Smith, 1970. Measurements of Spectral Irradiance Underwater. Gordon and Breach Publishers, New York. 103 p.

Table 1

Apparent Optical Characteristics of Clear Ocean Water (Tyler et al., 1972) and Turbid San Vicente Water (Tyler and Smith, 1970)

	Clear Oceanic			San Vicente		
Wavelength (nm)	$K_t(m^{-1})$	$B_d \times 10^{-3}(m^{-1})$	$R_I \times 10^{-2}(d=\infty)$	$K_t(m^{-1})$	$B_d \times 10^{-3}(m^{-1})$	$R_I \times 10^{-2}(d=\infty)$
450	0.111	5.160	4.649	2.403	112.2	4.670
460	0.112	4.760	4.250	2.169	108.7	5.010
470	0.113	4.352	3.851	1.955	116.1	5.940
480	0.114	3.931	3.448	1.751	122.2	6.980
490	0.116	3.364	2.900	1.620	121.2	7.480
500	0.124	2.852	2.300	1.526	121.6	7.970
510	0.139	2.360	1.698	1.397	123.2	8.820
520	0.147	2.058	1.400	1.277	131.3	10.280
530	0.156	1.872	1.200	1.149	127.3	11.080
540	0.164	1.640	1.000	1.106	124.0	11.210
550	0.178	1.511	0.849	1.049	116.3	11.090
560	0.192	1.400	0.729	0.997	112.9	11.320
570	0.220	1.298	0.590	0.978	111.9	11.440
580	0.266	1.197	0.450	0.977	112.0	11.360
590	0.346	1.125	0.325	1.067	104.9	9.830
600	0.486	1.021	0.210	1.235	100.1	8.170
610	0.550	0.935	0.170	1.268	88.9	7.010
620	0.604	0.876	0.145	1.300	86.3	6.610
630	0.662	0.768	0.116	1.329	79.7	6.000
640	0.720	0.619	0.086	1.341	75.0	5.590
650	0.790	0.490	0.062	1.407	68.4	4.860
660	0.860	0.344	0.040	1.621	58.0	3.580
670	0.940	0.207	0.022	1.756	58.5	3.330
680	1.010	0.101	0.010	1.762	67.8	3.850
690	1.100	0.055	0.005	1.793	63.3	3.530
700	1.260	0.025	0.002	2.009	55.2	2.750

TABLE 2

Counts/Radiance Conversion Constants for LANDSAT-4 TM bands 1, 2 and 3 (Barker et al., 1983) and LANDSAT-3 MSS bands 4 and 5 (Bauer, 1980).

	Dynamic Range		
	R_{min}*	R_{max}**	Gain
Band	(mw/cm^2-str-μm)		(counts/mw/(cm^2-str-μm))
TM 1	-0.152	15.842	15.78
TM 2	-0.284	30.817	8.10
TM 3	-0.117	23.463	10.62
MSS 4	0.4	22.0	5.79
MSS 5	0.3	17.5	7.27

* Largest radiance value observed for a count value of 0.
** Smallest radiance value observed for a TM count value at 255 or an MSS count value of 126.

Table 3

SQI VALUES* AND APPARENT CONTRAST** BETWEEN SAV AND SAND FOR THE CASE OF CLEAR OCEAN WATER

Band	d=0.5m		d=1.5m		d=10.0m	
	SQI	ΔC	SQI	ΔC	SQI	ΔC
TM 1	143.8	16.3	128.9	14.4	49.2	5.2
TM 2	101.4	5.6	79.9	4.3	12.5	0.6
TM 3	235.8	14.0	120.7	6.0	0.1	0.0
MSS 4	108.2	3.7	88.1	2.9	18.6	0.6
MSS 5	214.1	8.2	117.4	3.8	0.5	0.0

* Units = $(mw/cm^2\text{-str-nm})^{1/2} \times 10^{-3}$
** Units = Counts

Table 4

SQI VALUES* AND APPARENT CONTRAST** BETWEEN SAV AND MUD FOR THE CASE OF CLEAR OCEAN WATER

Band	d=0.5m		d=1.5m		d=10.0m	
	SQI	ΔC	SQI	ΔC	SQI	ΔC
TM 1	70.5	7.5	62.9	6.7	23.4	2.4
TM 2	2.8	0.4	1.8	0.1	4.2	0.1
TM 3	151.8	7.9	74.5	3.4	0.01	0.0
MSS 4	13.23	.6	8.5	0.5	0.2	0.1
MSS 5	127.5	4.3	67.9	2.0	0.2	0.0

* Units = $(mw/cm^2\text{-str-nm})^{1/2} \times 10^{-3}$
** Units = Counts

Table 5

SQI VALUES* AND APPARENT CONTRAST** BETWEEN SAV AND SAND
FOR THE CASE OF TURBID SAN VICENTE WATER

Band	d=0.5m		d=1.5m		d=10.0m	
	SQI	ΔC	SQI	ΔC	SQI	ΔC
TM 1	69.4	7.3	31.5	1.4	14.4	0.0
TM 2	70.6	3.7	42.8	1.2	25.6	0.0
TM 3	174.3	9.9	88.9	2.1	43.3	0.0
MSS 4	71.7	2.3	42.1	0.7	24.5	0.0
MSS 5	154.8	5.8	83.1	1.3	42.1	0.0

* Units = $(mw/cm^2\text{-}str\text{-}nm)^{1/2} \times 10^{-3}$
** Units = Counts

Table 6

SQI VALUES* AND APPARENT CONTRAST** BETWEEN SAV AND MUD
FOR THE CASE OF TURBID SAN VICENTE WATER

Band	d=0.5m		d=1.5m		d=10.0m	
	SQI	ΔC	SQI	ΔC	SQI	ΔC
TM 1	70.5	3.3	62.9	0.6	23.4	0.0
TM 2	3.1	0.3	1.6	0.1	0.8	0.0
TM 3	109.0	5.6	53.5	1.2	25.5	0.0
MSS 4	8.5	0.4	4.3	0.1	2.2	0.0
MSS 5	91.4	3.0	46.7	0.7	23.3	0.0

* Units = $(mw/cm^2\text{-}str\text{-}nm)^{1/2} \times 10^{-3}$
** Units = Counts

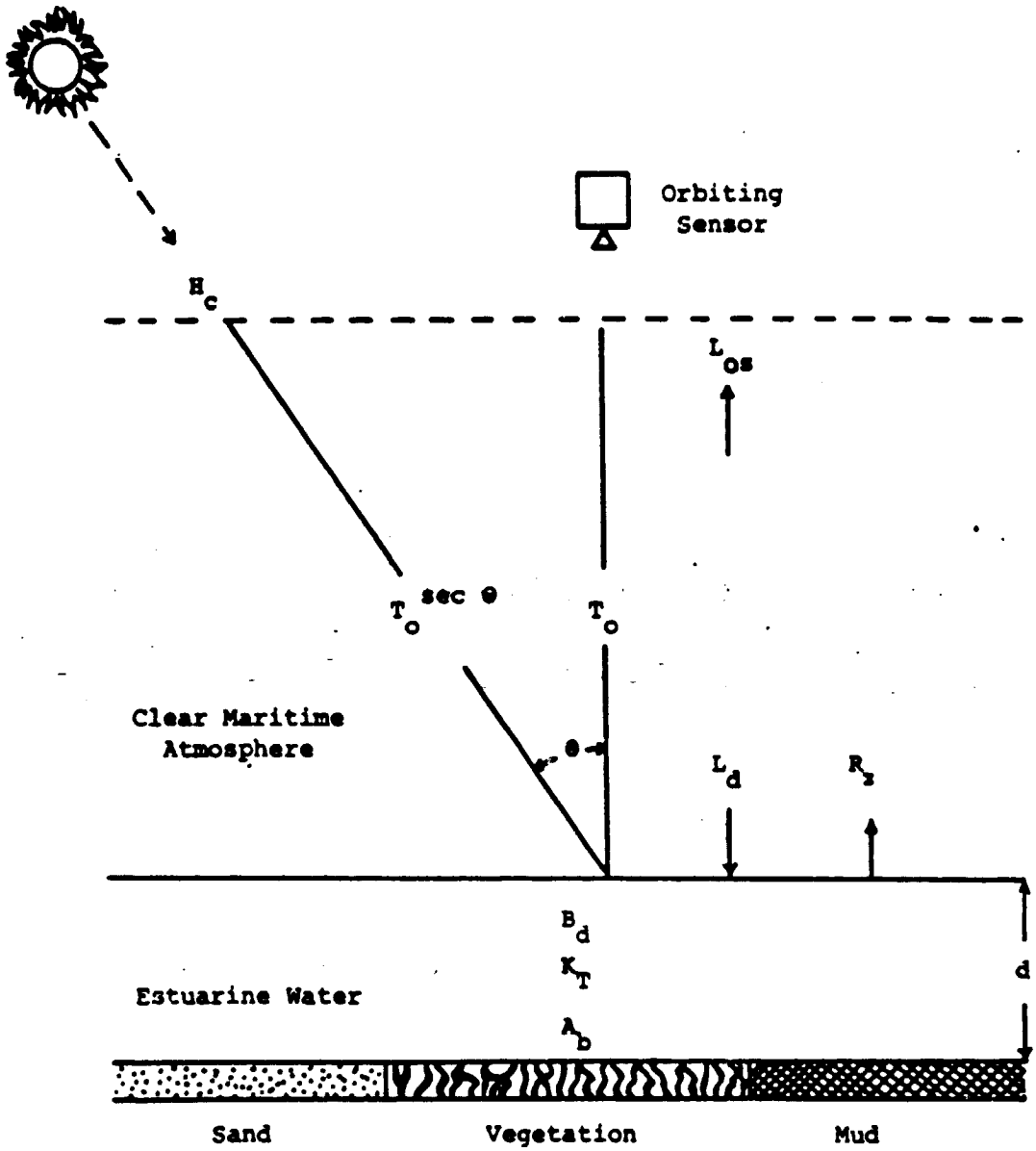

Figure 1. Optical parameters associated with radiative transfer within the estuarine environment.

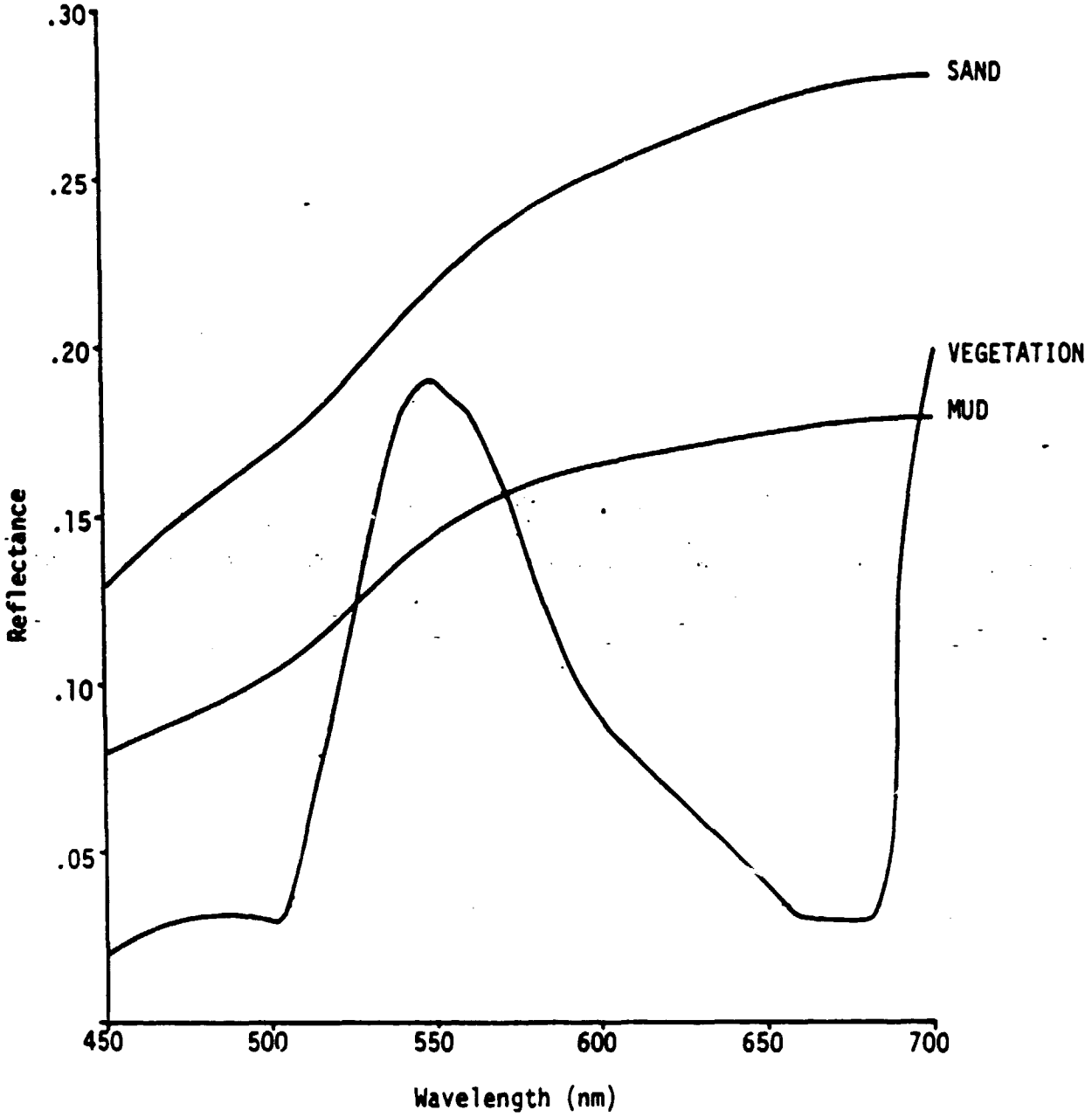

Figure 2. Irradiance reflectance of three bottom types used in the water reflectance model (Philpot, 1981). Sand = beach sand (Lyzenga and Thomson, 1978), mud = dark soil (Lyzenga and Thomson, 1978), and vegetation = an infinitely deep Ilex canopy (Gates et al, 1965).

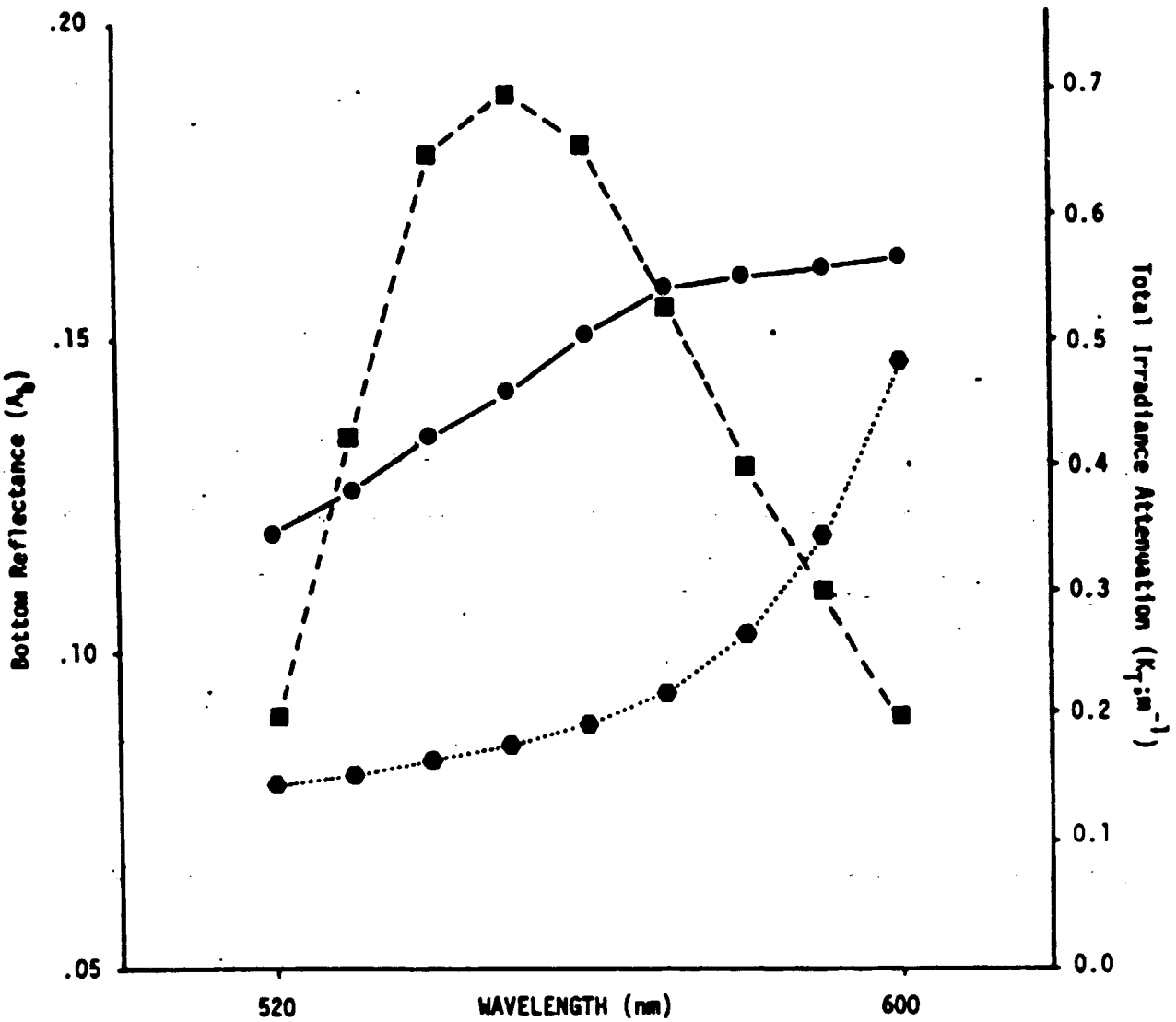

Figure 3. Irradiance reflectance of vegetation (■--■) and mud (●—●) and total irradiance attenuation for clear ocean water (●---●) plotted versus wavelength over TM band 2.

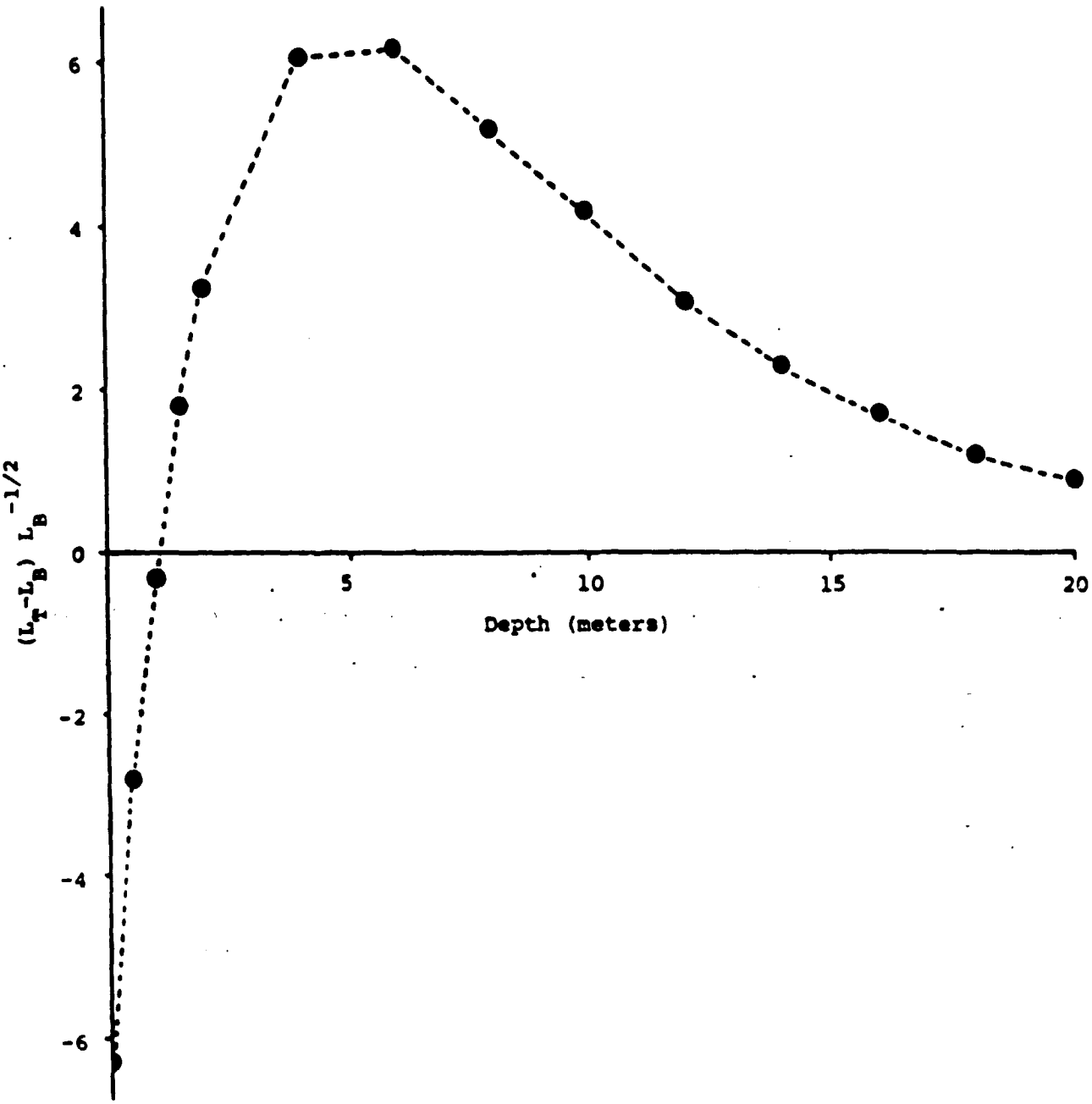

Figure 4. SQI values calculated without the absolute value of the numerator for TM band 2. The water type is clear ocean, L_T is the signal representing submerged vegetation, and L_B is the background signal representing a bottom of mud.

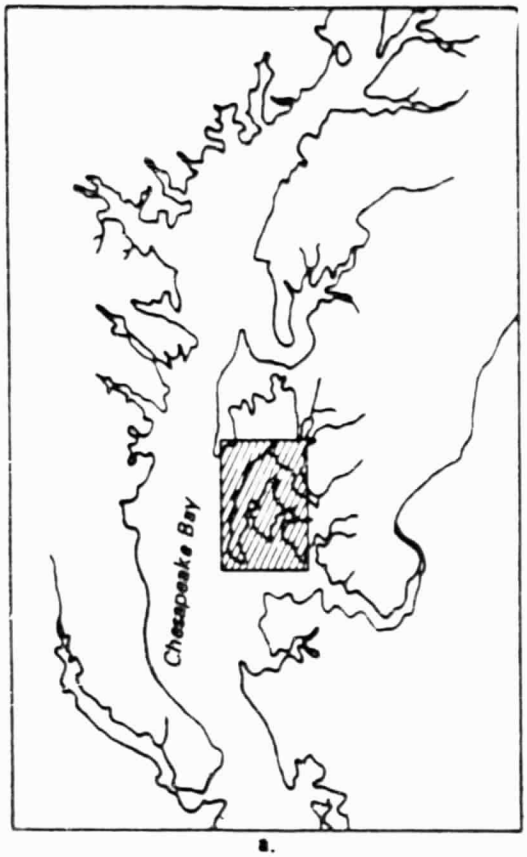

a.

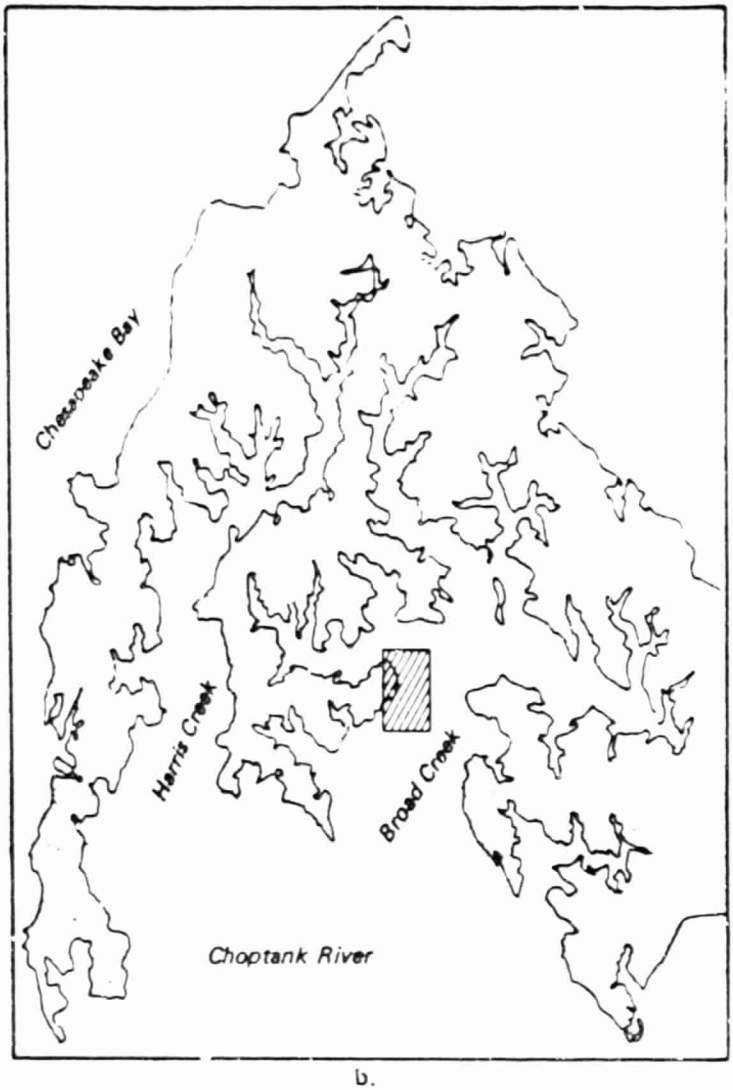

b.

FIGURE 5.

A portion of Chesapeake Bay is shown in plate a and an enlarged portion of Broad Creek, Maryland appears in plate b. The boxed area within plate b was photographed from low altitude on August 2, 1982. The photograph, plate c, shows a medium size SAV bed adjacent to the shoreline.

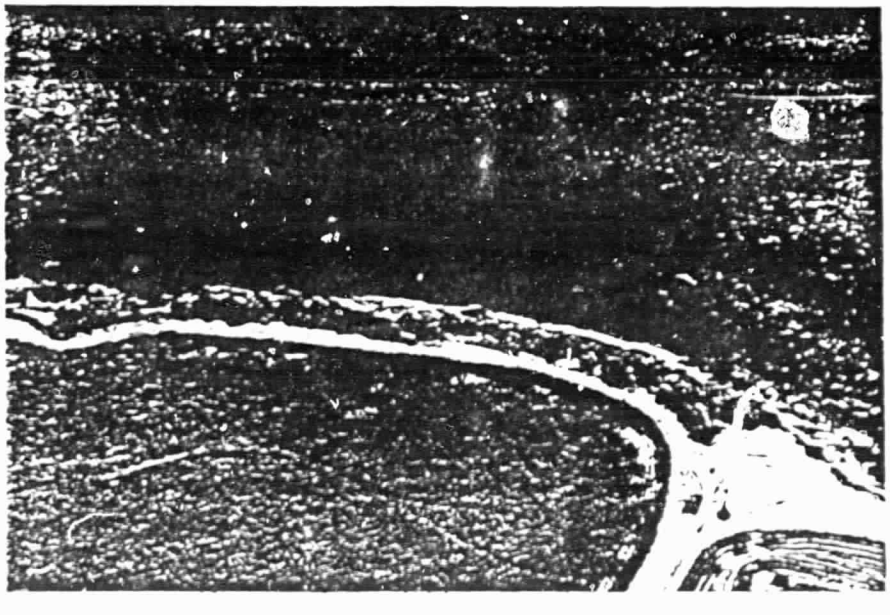

c.

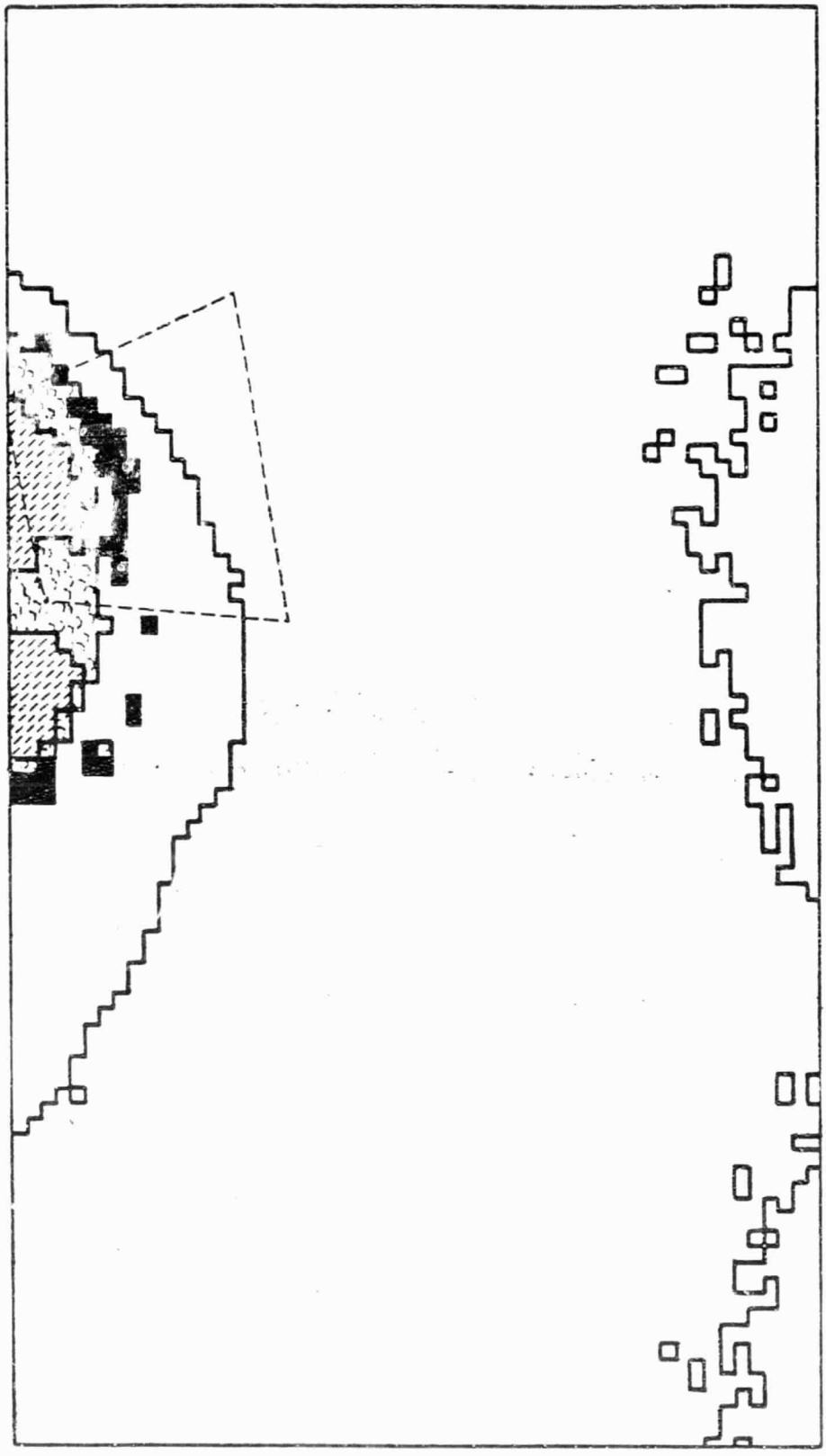

FIGURE 6.

A portion of the November 2, 1982 TM image classified using an ERDAS 400 microcomputer and an unsupervised clustering routine. The dashed lines represent the area photographed from low altitude and shown in Figure 5c. Pixels classified as SAV are shown as ■, optically deep water as □, submerged sand as □, and land as either ▨ (fields) or ▨ (trees).

REMOTE SENSING OF COASTAL WETLANDS BIOMASS USING THEMATIC MAPPER WAVEBANDS

Michael A. Hardisky
Vytautas Klemas

College of Marine Studies
University of Delaware
Newark, Delaware 19711

ABSTRACT

Spectral data, simulating thematic mapper bands 3, 4 and 5 were gathered in salt and brackish marshes using a hand-held radiometer. Simple regression models were developed equating spectral radiance indicies with total live biomass for S. alterniflora in a salt marsh and for a variety of plant species in a brackish marsh. Models were then tested using an independent set of data and compared to harvest estimates of biomass. In the salt marsh, biomass estimates from spectral data were similar to harvest biomass estimates during most of the growing season. Estimates of annual net aerial primary productivity calculated from spectral data were within 21% of production estimated from harvest data. During August, biomass estimates from spectral data in the brackish marsh were similar to biomass estimated by harvesting techniques. At other times during the growing season, spectral data estimates of biomass were not always comparable to harvest biomass estimates. Reasonable estimates of wetlands biomass are possible during the peak of the growing season (August) using spectral data similar to thematic mapper bands 3, 4 and 5 gathered with hand-held radiometers.

INTRODUCTION

Basic to the understanding of wetland function and value is the quantification of energy fixation. Reduced carbon compounds comprising macrophytic biomass provide the energy necessary to maintain the heterotrophic organisms which feed upon them. Aboveground biomass represents only a portion of total net primary production (belowground production can also be substantial) however, the fixed carbon in this biomass is the surplus available to heterotrophic organisms and is readily detected with remote sensing devices.

Presented at the Landsat-4 Science Characterization Early Results Symposium, NASA Goddard Space Flight Center, Greenbelt, MD, 23-24 February 1984. NASA Conference Publ. IV:251-269.

Many salt marshes on the eastern coast of the U.S. are dominated by a single plant Spartina alterniflora, Loisel. (Reimold 1977). S. alterniflora biomass can vary from near 100 to over 3000 gdw m^{-2} depending upon substrate type, soil salinity, inundation frequency or other edaphic factors. As interstitial water salinity decreases to the 18-15°/$_{oo}$ range, S. alterniflora is gradually replaced by a variety of plant species. In general, the lower the salinity, the greater the diversity of the resident plant population. The monospecific gramineous canopies of the salt marsh are transformed to brackish marsh canopies comprised of mixtures of gramineous, broadleaf and leafless plants. Spatially and temporally the canopies encountered in the brackish system are complex and dynamic. The morphologic diversity of the plant community produces an equally diverse spectral signature.

The study described herein was designed to develop simple regression models equating spectral radiance indicies with plant biomass. The radiance data were spectrally similar to thematic mapper bands 3, 4 and 5 and have been suggested as being superior to MSS wavebands for vegetation monitoring (Tucker 1978). Our first objective was to use these models to predict biomass and net primary productivity for a salt marsh and to predict biomass for a brackish marsh using ground gathered spectral radiance data. Our second objective was to assess the validity of our biomass estimation by comparing the spectrally estimated biomass values with biomass estimates obtained by traditional harvest techniques.

METHODS

Salt Marsh

A portion of the Canary Creek salt marsh in Lewes Delaware was selected for study (Figure 1). The marsh was dominated by monospecific stands of S. alterniflora with relatively small areas of Distichlis spicata (L.) Greene. Occassionally, Salicornia europaea L. or Limonium sp. occurred mixed with S. alterniflora. Six transects extending from the creek edge to the upland were established. The transects were spaced approximately 210 meters apart and stations were designated every 30m along each transect. A total of 40 stations for the whole marsh were established. By establishing stations in a systematic manner along transects, we sampled a representative cross section of S. alterniflora height forms occurring within the marsh. Beginning on 15 May 1981 and continuing every three weeks until 9 October 1981, four stations were selected, using a table of random numbers, from each transect. For each of the eight sampling dates, 24 stations were sampled yielding a total of 192 for the season.

Brackish Marsh

A brackish marsh near the headwaters of Old Mill Creek at Lewes, Delaware was selected for study (Figure 1). The interstitial water salinity varied from approximately 15-18°/$_{oo}$ at the downstream end to about 12-10°/$_{oo}$ at the upstream end. Plant species comprising the plant community changed with apparent soil salinity. Four transects extending from the creek edge to the upland were established 180 meters apart

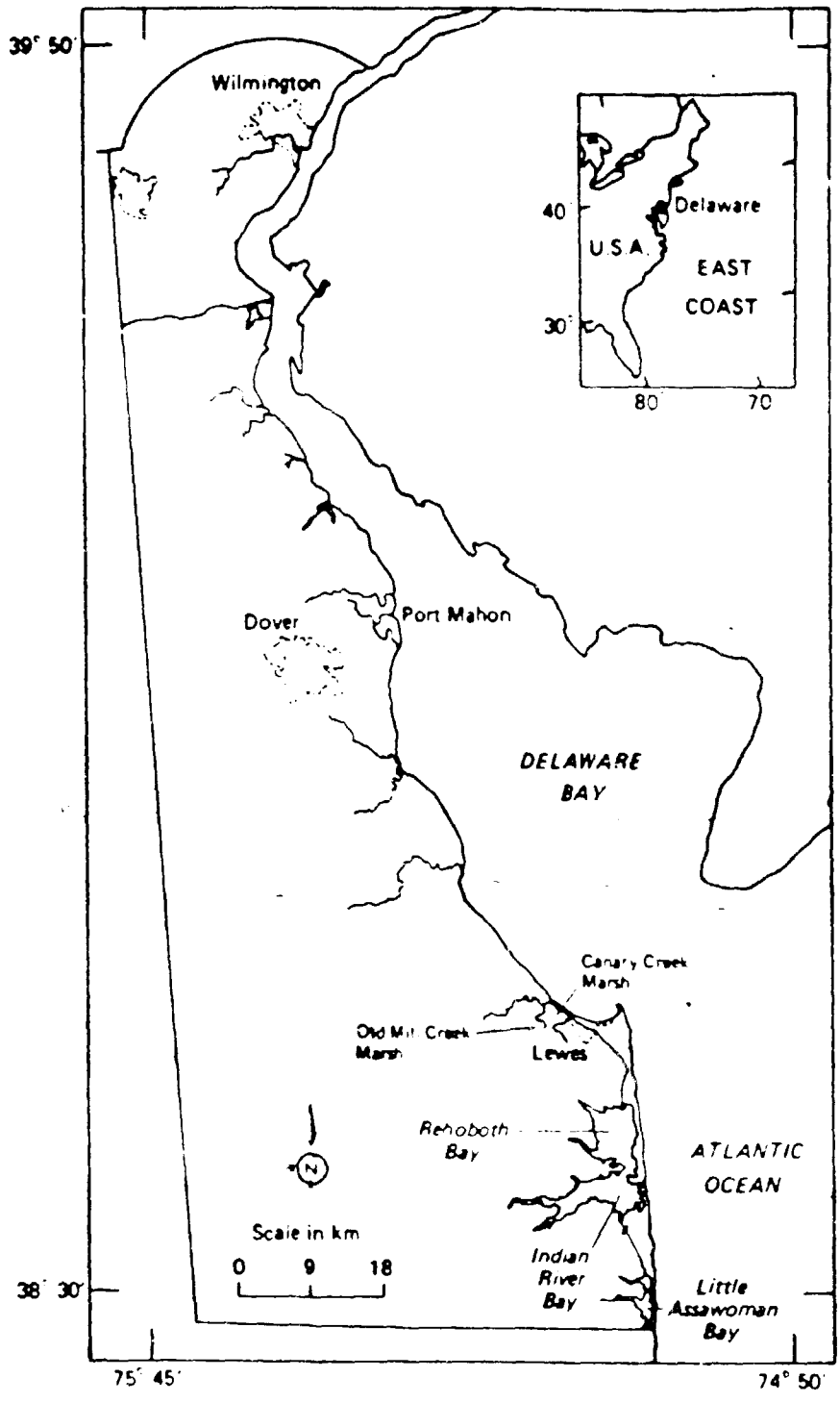

Fig. 1 Location of salt and brackish marsh test sites near Lewes, Delaware.

along the long axis of the creek. Stations were spaced at 30m intervals along each transect. A total of 29 stations were designated in the marsh. The marsh was sampled 3 times during the growing season (June, August, September) at approximately 6 week intervals. At each sampling date, 4 stations were selected using a table of random numbers from each transect yielding 16 stations and a season total of 48.

Spectral Radiance Data Collection

Before harvesting, a GSFC Mark II hand-held radiometer (Tucker et al. 1981a) was used to measure canopy radiance directly over each area to be harvested. The radiometer contained three wavebands spectrally configured with interchangeable interference filters to match bands 3, 4 and 5 of the Landsat-4 thematic mapper. The sensor head housed a red band (0.63 - 0.69 μm, RED) sensitive to chlorophyll concentration, a near infrared band (0.76 - 0.90 μm, NIR) sensitive to plant tissue structure or biomass and a middle infrared band (1.55 - 1.75 μm, IR) sensitive to leaf moisture. Data were recorded simultaneously for all three bands.

No more than 5 days prior to the actual harvest, spectral radiance was determined for each plot. The radiometer was leveled approximately 1.5 meters above the top of the plant canopy. In the brackish marsh a wooden step ladder was employed to achieve proper instrument height. The radiance was measured 3 times over each plot. Radiance data were not collected under cloudy or very windy conditions and were always collected within 2 hours of solar noon. Radiance data were collected during low tide, however, there were occasions when small amounts of tidal water remained pooled on the marsh. Standing water was avoided whenever possible due to potential specular reflectance from the water surface.

Spectral radiance data were transformed and expressed as a normalized difference of two bands as outlined by Kriegler et al. (1969) and Rouse et al. (1973). The red and near infrared radiance values were combined in the following manner:

$$VI = \frac{NIR - RED}{NIR + RED}$$

where VI is the vegetation index, NIR is the near infrared band radiance and RED is the red band radiance. A similar combination of the near infrared and middle infrared bands was performed (middle infrared substituted for RED in the above expression) and termed the infrared index (II). The infrared index is used here with the understanding that the near infrared and the middle infrared bands are spectrally different and that normalization in this manner may not be totally valid since adjacent, spectrally similar bands were assumed for this transformation (Kriegler et al. 1969). Index values were preferred to raw radiance data because the normalization procedure tends to compensate for changes in solar irradiance caused by seasonal changes in solar zenith angle and/or atmospheric conditions (Tucker et al. 1979a).

Harvesting Procedures

After collection of radiance data, all vegetation (including standing dead material) within a 0.25 m^2 frame was clipped at soil level at each station. The plant material was bagged and returned to the laboratory for processing. A 1/3 subsample (by wet weight) was drawn from the salt marsh samples and sorted into live and dead components. The brackish marsh samples were sorted completely by species, then only plant species with a large volume of material were subsampled and finally live and dead components determined for each species. Most plants in the brackish marsh samples contained little attached dead so the majority of the dead material was considered as a composite of the whole sample. The subsampling procedure for both marsh types greatly reduced processing time. We felt that a representative subsample was sufficient to determine relative proportions of live and dead tissue and by retaining the entire 0.25 m^2 sample for biomass determination, we preserved the best estimate of biomass, given the oftentimes spatially heterogeneous distribution of biomass within the area sampled. Proportions of live and dead tissue determined from the subsample were then extrapolated to the entire biomass sample. All plant material was dried at 60°C to a constant weight, weighed to the nearest 0.1g and expressed as grams dry weight per square meter (gdw m^{-2}).

RESULTS

Salt Marsh - Biomass Estimation

Regression models equating S. alterniflora biomass and spectral radiance indicies were developed during the 1980 growing season (Hardisky et al. 1983a). These models included short and tall form S. alterniflora sampled from June through November using the hand-held radiometer. Table 1 lists the models for the vegetation and infrared indicies. To estimate live and dead biomass, one solves for live leaf biomass (L) in the first equation, for total live biomass (live leaves and stems, T) in the second equation and then substitutes the L value (from equation 1) into the last equation solving for dead biomass (D). Through this sequence, the necessary parameters for annual net aerial primary productivity estimation (total live biomass and dead biomass) are calculated.

Figure 2 depicts biomass estimates from harvesting and computed from the vegetation index for S. alterniflora. For live and total biomass, the predicted values were similar to the harvest values throughout the year. Live biomass estimates using the vegetation index tended to be lower than harvest estimates during the first half of the growing season and were higher than harvest estimates during the latter half of the growing season. Peak biomass was attained in early August at which time canopy development would be the fullest. We would expect the greatest proportion of live biomass compared to dead biomass to occur at this time and for the greatest amount of live tissue to be in the upper portions of the canopy. This may have contributed to the higher vegetation index biomass estimates seen at peak biomass and thereafter. Dead biomass did not vary greatly over the season (from 260 to 400 gdw m^{-2}) however, decomposition of carry-over dead material (from previous growing

season, high in the canopy) and the concurrent addition of dead material from immature culm mortality and leaf senescence (low in the canopy) can change the relative vertical position of the dead biomass without large changes in biomass thereby altering reflectance from this component. It would seem reasonable that this change in the location of dead material contributed to the lower live biomass predictions in the first part of the season (when more dead material was in the canopy) and to the higher live biomass predictions in the latter part of the season (when less dead material was in the canopy).

Table 1

REGRESSION MODELS FOR PREDICTING S. ALTERNIFLORA BIOMASS

Regression Model	Coefficient of Determination (r^2)
VI = .382 + .068 ln(L)	0.75
VI = .149 + .096 ln(T)	0.64
VI = .760 + .055 ln(L/D)	0.88
II = .178 + .104 ln(L)	0.87
II =-.185 + .148 ln(T)	0.76
II = .752 - .078 ln(L/D)	0.88

L - Live leaf biomass: T - Total live biomass; D - Dead biomass
Units on all biomass = grams dry weight per meter squared
n for all regression models = 96
VI = Vegetation Index; II = Infrared Index

Harvest and infrared index estimates of live and total S. alterniflora biomass are compared in Figure 3. The infrared index estimates of live biomass were very close to the harvest estimates during the early part of the growing season. After peak biomass, the infrared index estimates of live biomass were lower than harvest estimates. The reasons for the apparent underestimates at the end of the growing season are not clear, however, we would postulate that the lower water content of the plant tissue due to tissue maturity and increased interstitial water salinity at this time in the growing season would cause an increase in the middle infrared reflectance resulting in lower infrared index values. Overall the infrared index and vegetation index estimates of biomass were similar.

Although the mean biomass estimates from harvesting and from radiance indicies were similar, considerable variability existed for individual measurements during some parts of the growing season. Figure 4 presents coefficients of determination (r^2) between harvest estimates and vegetation or infrared index estimates of live (a) and total (b) biomass. High r^2

values indicate good linear association between individual harvest and radiance index estimates of biomass. Low r^2 values indicate considerable variation existed for some samples between the two biomass estimates. From May through June, the most disagreement between harvest and radiance index biomass estimates existed. August was the best time period for agreement of the biomass estimates with the latter part of the growing season as a whole being better than the first part. The harvest and radiance index estimates of live biomass were always in better agreement than the total biomass estimates. Harvest and radiance index biomass means in Figures 2 and 3 were generally very similar. This suggests that during those periods when low r^2 values existed between harvested and predicted biomass, the amount of overestimation and underestimation were similar among the 24 samples, yielding means which were comparable. When using radiance index values for biomass prediction, one should scrutinize the results from individual measurements to assure that each estimate is reasonable, particularly early in the growing season.

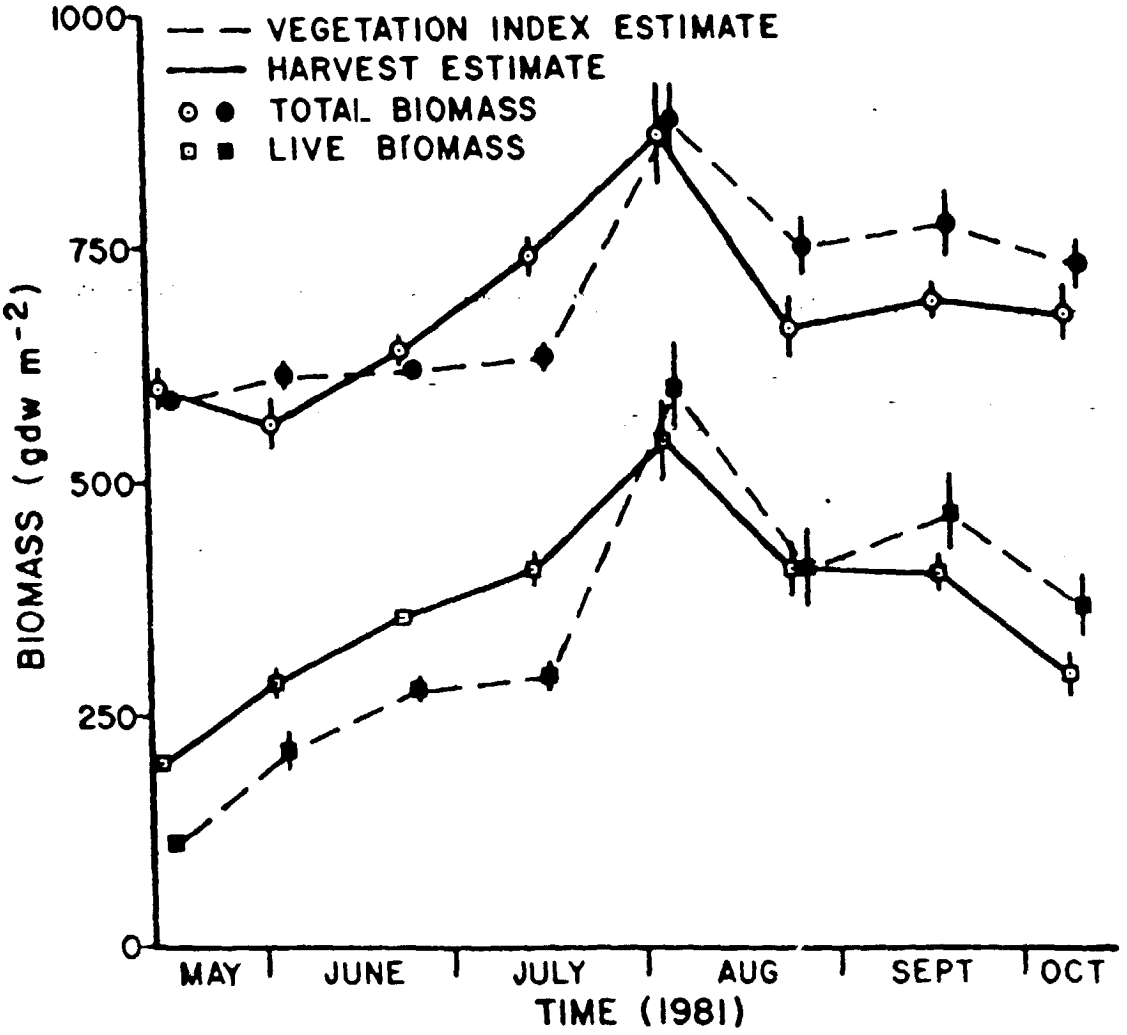

Fig. 2 Vegetation index and harvest estimates of S. alterniflora biomass over the growing season. Bars representing 1 standard error of the mean are shown whenever they exceed the size of the point symbol. Points are slightly offset to improve readability.

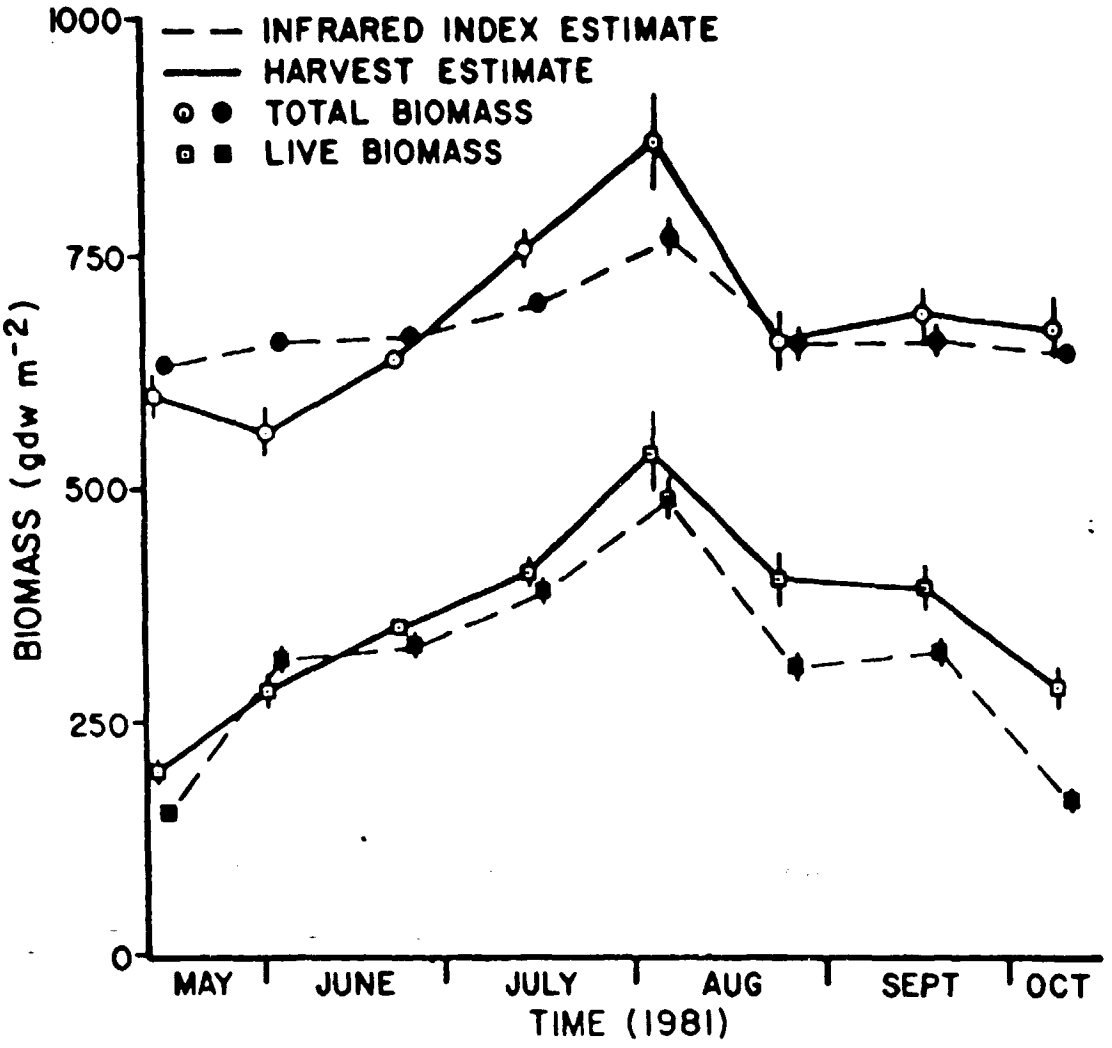

Fig. 3 Infrared index and harvest estimates of S. alterniflora biomass over the growing season. Bars representing 1 standard error of the mean are shown whenever they exceed the size of the point symbol. Points are slightly offset to improve readability.

Salt Marsh - Productivity Estimation

Using the mean biomass estimates shown in Figures 2 and 3, annual net primary productivity was computed for the S. alterniflora salt marsh. We employed established production calculation techniques used widely in salt marsh systems (Table 2). There is some discussion as to the adequacy of these techniques and we recognize the shortcomings of each. However, these techniques are widely used and will yield values comparable to other studies. Linthurst and Reimold (1978) provide an excellent comparison of various harvest techniques for estimating net aerial primary productivity in estuarine marsh systems.

Annual net aerial primary productivity estimates for the Canary Creek marsh are found in Table 2. The vegetation index estimate of productivity was within 4% of the Smalley (1958) harvest technique and no more than 21% different from the other techniques. The infrared index estimates of productivity were within 20% of the Smalley (1958)

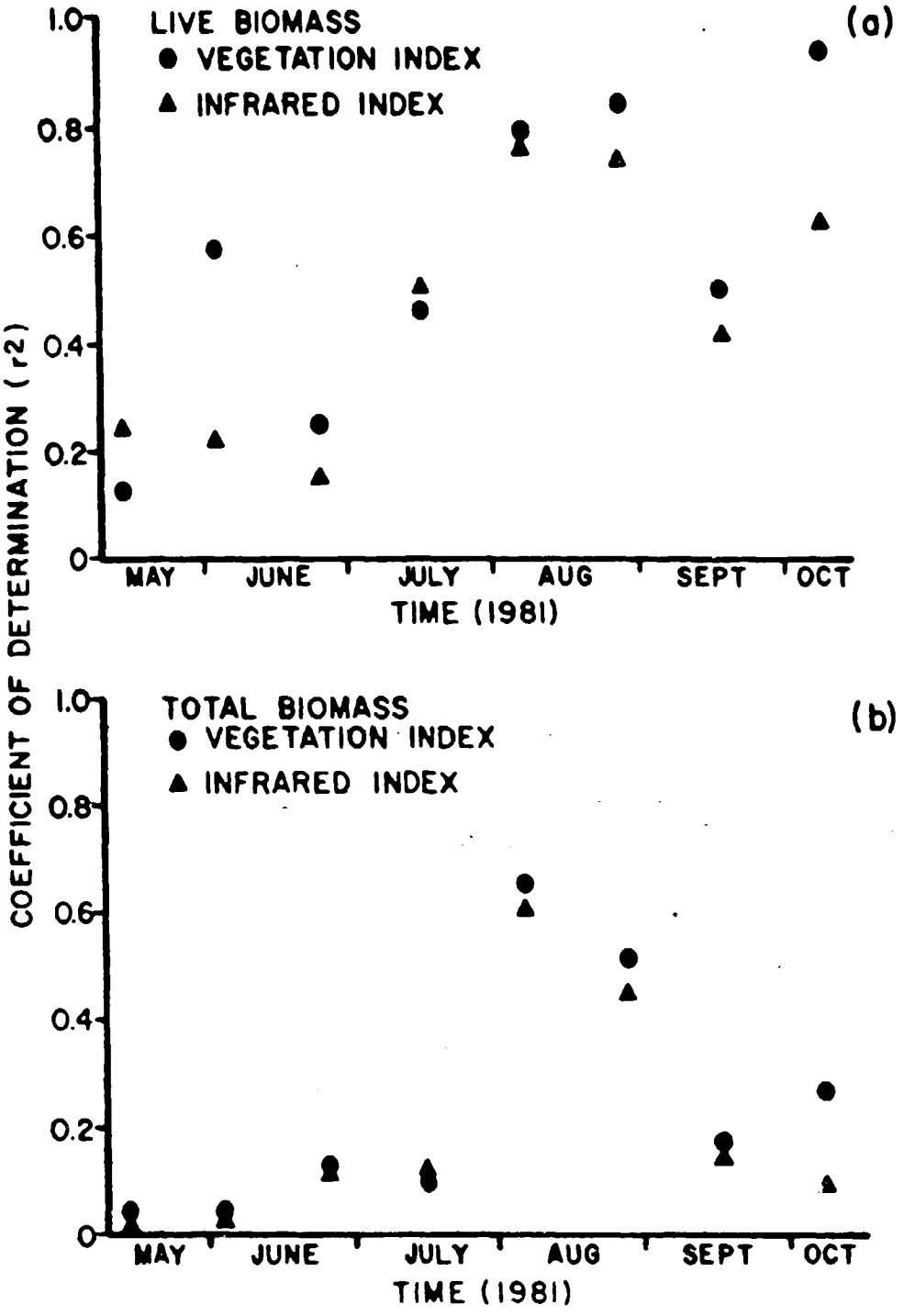

Fig. 4 Coefficients of determination describing the association between radiance index predictions of biomass and harvest estimates of biomass over the growing season.

technique and were 4-5% different from the other techniques. The key to the agreement between the productivity estimates computed from harvest and radiance index data was the high correlation between predicted and harvest biomass during peak biomass (August). For all but the peak standing crop method of production estimation, successive positive increments in biomass are summed throughout the growing season, normally culminating at the point of peak biomass. Therefore, the estimation of peak biomass is the single most critical measurement in determining annual production.

Table 2

ANNUAL NET AERIAL PRIMARY PRODUCTIVITY ESTIMATES
FOR SPARTINA ALTERNIFLORA IN CANARY CREEK MARSH

Method	Harvest Estimate	Remote Sensing Estimate	
		VI	II
peak standing crop	517	600	489
Milner & Hughes (1968)	523	661	498
Morgan (1961)	517	600	497
Smalley (1958)	634	661	506

all values are grams dry weight per square meter per year
VI = Vegetation Index; II = Infrared Index

Brackish Marsh - Model Development

Modeling the relationship between spectral radiance indicies and live aerial biomass in brackish marsh plant communities required consideration of diverse morphologic characteristics among plants residing in the same community. To illustrate this point, Figure 5 shows the linear relationship between vegetation index and live biomass for a variety of wetland plants. Iva, Polygonum, and Solidago represent broadleaf or deciduous canopies and exhibit rapid increases in vegetation index for relatively small changes in biomass. This characteristic suggests that the spectral index can become saturated rapidly. Structurally, these canopies maintain most leaf surfaces in the horizontal plane and generally form a complete canopy cover which reduces or eliminates exposure of dead components or soil background to solar irradiance. This combination of canopy characteristics yields a very absorptive canopy in the red region and a very reflective canopy in the near infrared region, thus the high vegetation index relative to the amount of live biomass present.

The opposite extreme to the broadleaf canopy would be the leafless canopies represented by Salicornia and Scirpus. Both Salicornia virginica and Scirpus olneyi possess erect, leafless stems with most green tissue in the vertical plane and primarily soil background and dead plant material in the horizontal plane. Normally these canopies are very open with soil

surface characteristics potentially contributing greatly to the observed spectral radiance.

The third canopy type represented in Figure 5 is the gramineous canopy type of Spartina and Typha. Spartina alterniflora exhibits alternate leaves along the length of the stem whereas Typha angustifolia has basal leaves. Both plants form canopies with portions of leaves in the horizontal and in the vertical plane. S. alterniflora exhibits a broad range of canopy configurations as a result of its wide environmental tolerance limits. Both plant canopies can maintain substantial quantities of dead material within the canopy. The amount of live leaf tissue determines to what degree dead material and soil background will influence spectral reflectance. Theoretically, the occurrance of flat leaves (portions of which may be horizontal) in the gramineous canopy would place them somewhere between the broadleaf and leafless canopies in terms of an increase in vegetation index value for an increase in biomass (i.e. an intermediate slope). In practice this does not occur because the measured vegetation index represents the composite of reflectance from vegetation (live and dead) and the soil. In the case of the gramineous canopy, the dead vegetation and soil are oftentimes well illuminated and contribute significantly to the measured vegetation index. The net effect is a lessening of vegetation index increases with increasing biomass.

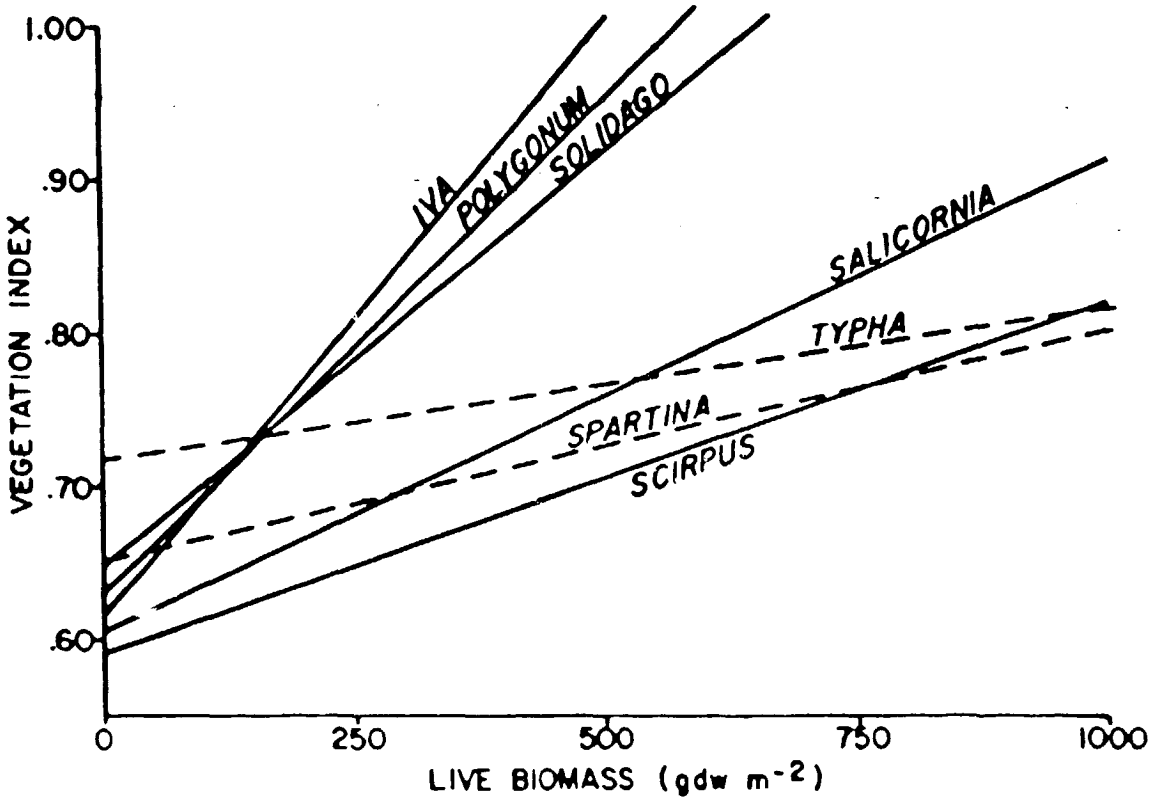

Fig. 5 Comparison of the relationship between vegetation index values and amounts of live biomass for a variety of wetland plants. Iva, Polygonum and Solidago represent broadleaf canopies, Typha and Spartina (dashed lines) represent gramineous canopies and Salicornia and Scirpus represent leafless canopies.

Brackish marsh plant communities are often composed of numerous plant species with morphologies represented by each of the groups discussed. The problem of equating spectral data with live biomass becomes a function of the species composition of the community in question. At present, we lack sufficient data for modeling specific mixtures of the 3 canopy types. So as a first attempt at equating spectral radiance indicies and live aerial biomass, we combined data from each of the morphologic groups into a single model. These data were gathered from stands of Typha angustifolia, Spartina alterniflora, Scirpus olneyi and a broadleaf mixture normally dominated by Acnida cannabina or Hibiscus moscheutos. The areas were sampled monthly from May through August with radiance and biomass data being gathered identical to the brackish marsh samples described in the methods.

Brackish Marsh - Biomass Estimation

The brackish marsh sampled for biomass estimation was diverse in terms of plant species and seasonally dynamic with respect to dominance. Table 3 lists the abundance (expressed as a percent of the total number of samples in which the plant species occurred) and dominance (expressed as a percent of the total number of samples in which the plant species was dominant in terms of biomass) of each plant species encountered during the study. The three most abundant species were Spartina patens, Eleocharis sp. and Acnida cannabina. Grass species dominated most samples during all three sampling periods. There was a slight increase in dominance by broadleaf species in August when most broadleaf plants reached peak biomass.

Simple and multiple regression models equating total live biomass (all species within sample) and the spectral radiance indicies with other canopy descriptors are found in Table 4. Multiple regression models were included for comparison because the percent of total live biomass which was broadleaf biomass (B) and total live biomass expressed as a percent of live plus dead biomass (P) were consistently implicated as important parameters for best fit models. Considering the very different spectral characteristics of broadleaf canopies relative to the gramineous and leafless canopies, and the potential importance of dead vegetation in determining spectral radiance in gramineous and leafless canopies, it was not surprising that these additional parameters (B,P) significantly improved the linear fit (r^2 values) of the models.

Harvest and spectral radiance index estimates of total live biomass for the entire growing season are compared in Table 4. In the case of the vegetation index, the inclusion of B and P reduced the accuracy of the biomass estimate, whereas with the infrared index these two parameters apparently improved the biomass estimate but not to any significant degree. The annual live biomass means predicted with radiance index data were very similar to the live biomass estimated by harvesting. A paired T-test suggested that most harvest and predicted means were not statistically separable at the 0.05 level.

Table 3

ABUNDANCE AND DOMINANCE OF PLANT SPECIES COMPRISING THE OLD MILL CREEK BRACKISH MARSH

Plant Species	June		August		September	
	Abundance[a] (%)	Dominance[b] (%)	Abundance (%)	Dominance (%)	Abundance (%)	Dominance (%)
Acnida cannabina L.	44	6	63	25	44	0
Aster tenuifolius L.	6	0	19	0	25	0
Atriplex patula L.	6	0	19	0	0	0
Carex lurida Wahl.	13	0	13	0	6	0
Distichlis spicata (L.) Greene	50	13	19	0	38	0
Eleocharis sp.	63	0	63	0	50	6
Hibiscus moscheutos L.	44	13	25	6	13	13
Iva frutescens L.	0	0	6	0	0	0
Kosteletzkya virginica (L.) Presl	0	0	13	6	0	0
Panicum virgatum L.	0	0	0	0	6	6
Pluchea purpurascens (Swartz) DC	0	0	0	0	6	0
Polygonum punctatum Ell.	38	0	25	0	19	0
Scirpus olneyi Gray	19	0	13	6	25	6
Spartina alterniflora Loisel.	31	19	44	19	31	25
Spartina cynosuroides (L.) Roth	13	6	19	13	6	6
Spartina patens (Ait.) Muhl.	81	44	69	19	56	38
Unidentified grass	19	0	6	0	6	0

[a]Abundance is based upon presence or absence within a sample and expressed as a percent of the total plots harvested.

[b]Dominance is based upon biomass and expressed as a percent of the total plots harvested.

Table 4

REGRESSION MODELS EQUATING RADIANCE INDICES AND BRACKISH MARSH CANOPY PARAMETERS.

Model[a]	Annual Live Biomass (gdw m^{-2})		
	Harvest[b]	Predicted	Difference
T = (3278) VI - 1939	691(68)	647(33)	45
T = (4319) VI - (7.12)B - 2682	691(68)	550(49)	142*
T = (4025) VI - (7.16)B + (1.85)P - 2562	691(68)	553(49)	138*
T = (3877) II - 2181	691(68)	727(45)	36
T = (4242) II - (4.06)B - 2402	691(68)	680(51)	12
T = (3902) II - (4.41)B + (2.35)P - 2294	691(68)	674(52)	18

[a] T = total live biomass (gdw m^{-2}), VI = vegetation index, II = infrared index, B = live biomass of broadleaf species expressed as a percent of total live biomass, P = total live biomass expressed as percent of total live and dead biomass, n for all models is 57.

[b] Values are the mean and one standard error, in parenthesis, of 47 samples. Difference = the numerical difference between the harvest and predicted means. An asterisk indicates the difference between means was statistically significant at the 0.05 level.

The regression models were then used to estimate biomass at each of the 3 sampling dates (Table 5). Although there was good agreement between annual harvest and predicted biomass means, substantial deviation was noted over the growing season. Vegetation index biomass estimates were very good during June and August but unacceptable during September. The infrared index only produced acceptable biomass estimates during August. The failure of the models to yield good biomass estimates during September was probably related to the rapid senescence of the marsh plants at this time. The brackish marsh, unlike the salt marsh, contains annual broadleaf plants which after seed production senesce rapidly. The larger amount of dead vegetation in the canopy and the senescence of broadleaf leaves altered the canopy spectral characteristics sufficiently to invalidate the predictive models at this time of year. The infrared index estimates of biomass were high in June and low in September. The high percentage of moisture in young, productive leaf tissue (June) as opposed to the low percentage of moisture in dead or senescing leaf tissue (September) probably contributed to the observed fluctuations in biomass estimation for the infrared index.

Table 5

COMPARISON OF LIVE BIOMASS ESTIMATES FOR A BRACKISH MARSH BY MONTH

Variables[a] in Model	29 June 1981			12 August 1981			19 September 1981		
	Harvest[b]	Predicted	Diff.	Harvest	Predicted	Diff.	Harvest	Predicted	Diff.
VI	609(113)	739(54)	130	649(80)	697(49)	48	814(148)	507(55)	307*
VI, B	609(113)	678(55)	70	649(80)	585(64)	64	814(148)	387(110)	427*
VI, B, P	609(113)	674(56)	66	649(80)	590(66)	60	814(148)	398(111)	416*
II	609(113)	876(48)	267*	649(80)	772(76)	123*	814(148)	537(84)	277*
II, B	609(113)	846(47)	238*	649(80)	712(78)	62	814(148)	484(107)	330*
II, B, P	609(113)	828(52)	220*	649(80)	707(79)	58	814(148)	488(109)	326*

[a] VI = vegetation index, II = infrared index, B = live biomass of broadleaf species expressed as a percent of total live biomass, P = total live biomass expressed as a percent of total live and dead biomass.

[b] Values are the mean and one standard error, in parenthesis, of 16 samples. Values are live biomass (gdw m^{-2}). Diff. = the difference between harvest and predicted means. An asterisk indicates the difference between means was statistically significant at the 0.05 level.

DISCUSSION

Other investigators have found good correlations between marsh plant biomass and reflectance in the red and near infrared spectral regions (Drake 1976, Bartlett and Klemas 1981). We have reaffirmed this relationship for S. alterniflora using thematic mapper bands 3 and 4. Previous studies in salt marshes (Budd and Milton 1982), pasture land (Curran 1982) and in agricultural vegetation (Tucker et al. 1981b) suggest a strong relationship between plant biomass and the combination of red and near infrared spectral data. These studies also imply that biomass could be predicted using spectral data. Very few investigators have actually tested models equating biomass and spectral data using a data set independent of the data set used to establish the model. Jensen (1980) working with the salt marsh shrub (Halimione portulacoides) and Curran (1980) working with pasture vegetation have done this with reasonable success. Our data also suggest that spectral radiance models are useful for nondestructive estimates of salt marsh biomass.

The brackish marsh regression models predicted biomass well during the peak of the growing season. The models presented represent an oversimplification of the complex interactions of live and dead vegetation, horizontal and vertical leaf area index, and soil reflectance which are compressed and treated as a single reflecting surface. Brackish marsh canopies are normally much deeper and much more diverse in terms of plant morphologies than salt marsh canopies. It is, therefore, very encouraging when representatives of the 3 most common canopy types measured in relatively pure stands can be combined into a regression model which yields good estimates of biomass for mixed plant stands. The hypothesis that plant morphology (canopy type) is more important in determining measured spectral radiance than consideration of each particular plant species, appears to be valid. For example, Typha canopies were included as input to the predictive regression models, yet in the data set used to test the model, no Typha was present. On the other hand, many plant species were found in the test data set (notably S. patens, Eleocharis sp., D. spicata and P. punctatum) which were not included in the model development data set. The dissimilarities in species composition between the model development and model testing data sets apparently had little effect upon the outcome of live biomass predictions from radiance indicies.

The vegetation index was usually a better spectral transformation for biomass estimation than was the infrared index. The vegetation index has been well established as a useful transformation for monitoring vegetation (Tucker 1979, Tucker et al. 1979a,b) but the infrared index is relatively new. Kimes et al. (1981) and Markham et al. (1981) were among the first to work with the middle infrared band (TM5) using hand-held radiometry. In both studies, they concluded that the middle infrared band contained the same information as the red band. They did acknowledge that their sampling precluded any water stress and that the middle infrared band should undergo additional testing when changes in leaf moisture were expected. More recent work by Hardisky et al. (1983b) suggests that the infrared index may have moisture detection capabilities and therefore, will probably be useful in wetland systems for discriminating

vegetation exposed to varying soil salinity conditions. We believe that additional research must be conducted to determine the worth of the infrared index for vegetation monitoring. The large seasonal variation in biomass predictions in the brackish marsh by the infrared index suggest moisture content or the moisture contrast between live and dead vegetation may have contributed to the results. If our observations are a result of canopy moisture differences, this would indicate a larger seasonal fluctuation in canopy moisture relative to biomass than in chlorophyll content relative to biomass. This could potentially be a very useful tool in monitoring wetlands vegetation.

CONCLUSIONS

Regression models equating total live biomass and spectral radiance indicies were developed and tested for salt and brackish marsh vegetation. Comparisons of biomass predicted using spectral radiance indicies and biomass estimated by traditional harvest techniques were very similar for S. alterniflora biomass. The vegetation index was slightly better for predicting biomass than was the infrared index. The best agreement between predicted and harvested biomass occurred during August (at peak biomass) with a considerable amount of variability at other times of the year. Annual net aerial primary production estimates were also very similar using either predicted or harvest biomass estimates.

Three morphologically distinct canopy types were identified in the brackish marsh vegetation. Data gathered from broadleaf, gramineous and leafless canopies were combined into a single regression model for estimating brackish marsh biomass. The models provided similar estimates of biomass compared to harvest estimates of biomass during June and August for the vegetation index and only during August for the infrared index. Percent broadleaf biomass and percent live biomass were identified as being important parameters for determining total biomass with spectral data. In practice, these additional parameters did little to improve live biomass predictions over the live biomass predictions using only the spectral radiance index.

The thematic mapper bands 3, 4 and 5 used in this study successfully provided the spectral information necessary for nondestructive biomass estimates in coastal marshes. The ground-based radiometric technique described can provide the data necessary for estimates of productivity for some marsh systems. Spectral data gathered with hand-held radiometers from low altitude aircraft and thematic mapper simulator data are presently being tested using the models described in this paper. Preliminary results indicate that with an atmospheric correction, the models work well with spectral data gathered from higher altitude platforms. It seems plausible that the models presented here can be modified for use with thematic mapper spectral data.

ACKNOWLEDGMENTS

We thank Dr. Paul Wolf, Dr. Frank Daiber, Debbie Decker, Shirley Munsey, Dr. Charles Roman, Tom Hardisky, Paul Klemas, Andrew Klemas, Jon Pennock and Ricardo Soto for their assistance with the field work. We thank Mrs. Barbara MacKenzie for her secretarial expertise during manuscript preparation. This research was supported by NSF grant DAR-8017836 and by NASA grant NAS5-27580.

LITERATURE CITED

Bartlett, D. S. and V. Klemas. 1981. In situ spectral reflectance studies of tidal wetland grasses. Photogram. Eng. and Remote Sensing 47: 1695-1703.

Budd, J. T. C. and E. J. Milton. 1982. Remote sensing of salt marsh vegetation in the first four proposed Thematic Mapper bands. Int. J. Remote Sensing 3: 147-161.

Curran, P. 1980. Multispectral photographic remote sensing of vegetation amount and productivity. Proc. of the 14th International Sym. on Remote Sensing of Environment, Univ. of Michigan, Ann Arbor, pp. 623-637.

Curran, P. J. 1982. Multispectral photographic remote sensing of green vegetation biomass and productivity. Photogram. Eng. and Remote Sensing 48: 243-250.

Drake, B. G. 1976. Seasonal changes in reflectance and standing crop biomass in three salt marsh communities. Plant Physiol. 58: 696-699.

Hardisky, M. A., R. M. Smart and V. Klemas. 1983a. Seasonal spectral characteristics and aboveground biomass of the tidal marsh plant, Spartina alterniflora. Photogram. Eng. and Remote Sensing 49: 85-92.

Hardisky, M. A., V. Klemas and R. M. Smart. 1983b. The influence of soil salinity, growth form and leaf moisture on the spectral radiance of Spartina alterniflora canopies. Photogram. Eng. and Remote Sensing 49: 77-83.

Jensen, A. 1980. Seasonal changes in near infrared reflectance ratio and standing crop biomass in a salt marsh community dominated by Halimione portulacoides (L.) Aellen. New Phytol. 86: 57-67.

Kimes, D. S., B. L. Markham, C. J. Tucker and J. E. McMurtrey III. 1981. Temporal relationships between spectral response and agronomic variables of a corn canopy. Remote Sensing of Environment 11: 401-411.

Kriegler, F. J., W. A. Malila, R. F. Nalepka and W. Richardson. 1969. Preprocessing transformations and their effects on multispectral recognition. Proc. Sixth International Symp. on Remote Sensing of Environment. Ann Arbor, Michigan. pp. 97-131.

Linthurst, R. A. and R. J. Reimold. 1978. An evaluation of methods for estimating the net aerial primary productivity of estuarine angiosperms. J. Appl. Ecol. 15: 919-931.

Markham, B. L., D. S. Kimes, C. J. Tucker and J. E. McMurtrey III. 1981. Temporal spectral response of a corn canopy. Photogram. Eng. and Remote Sensing 47: 1599-1605.

Milner, C. and R. E. Hughes. 1968. Methods for Measurement of the Primary Production of Grasslands. Blackwell, Oxford. 70 p.

Morgan, M. H. 1961. Annual angiosperm production on a salt marsh. Master's Thesis, University of Delaware, Newark, DE. 34 p.

Reimold, R. J. 1977. Mangals and salt marshes of eastern United States. In: V. J. Chapman, ed. Wet Coastal Ecosystems, Elsevier Scientific Publ. Co., Amsterdam. pp. 157-166.

Rouse, J. W., R. H. Hass, J. A. Schell and D. W. Deering. 1973. Monitoring vegetation systems in the Great Plains with ERTS. Third Earth Resources Technology Satellite-1 Symposium. NASA, pp. 309-317.

Smalley, A. E. 1958. The role of two invertebrate populations, Littorina irrorata and Orchelimum fidicinum in the energy flow of a salt marsh ecosystem. Ph.D. Dissertation, University of Georgia, Athens, GA, 126 p.

Tucker, C. J. 1978. A comparison of satellite sensor bands for vegetation monitoring. Photogram. Eng. and Remote Sensing 44: 1369-1380.

Tucker, C. J. 1979. Red and photographic infrared linear combinations for monitoring vegetation. Remote Sensing of Environment 8: 127-150.

Tucker, C. J., J. H. Elgin, Jr., J. E. McMurtrey III and C. J. Fan. 1979a. Monitoring corn and soybean crop development with hand-held radiometer spectral data. Remote Sensing of Environment 8: 237-248.

Tucker, C. J., J. H. Elgin, Jr. and J. E. McMurtrey III. 1979b. Temporal spectral measurements of corn and soybean crops. Photogram. Eng. and Remote Sensing 45: 643-653.

Tucker, C. J., W. H. Jones, W. A. Kley and G. J. Sundstrom. 1981a. A three-band hand-held radiometer for field use. Science 211: 281-283.

Tucker, C. J., B. N. Holben, J. H. Elgin and J. E. McMurtrey. 1981b. Remote sensing of total dry-matter accumulation in winter wheat. Remote Sensing of Environment 11: 171-189.